

# River floods in the Anthropocene impact sea-floor geochemistry, pollutants and bacterial communities in coastal systems

Claudio Pellegrini<sup>1</sup>, Marco Basili<sup>2</sup>, Irene Sammartino<sup>1\*</sup>, Tommaso Tesi<sup>3</sup>, Emanuela Frapiccini<sup>2</sup>, Grazia Marina Quero<sup>2-4</sup>, Sarah Pizzini<sup>2-5</sup>, Roberta Zangrando<sup>3</sup>, Gianmarco Luna<sup>2-4</sup>, Sara Catena<sup>1</sup>, Naomi Massaccesi<sup>2-4-6</sup>, Fabio Trincardi<sup>7</sup>, Andrea Gallerani<sup>1</sup>, Jacopo Chiggiato<sup>1</sup>.

<sup>1</sup>Consiglio Nazionale delle Ricerche, Istituto di Scienze Marine (CNR-ISMAR), Italy

<sup>2</sup>Consiglio Nazionale delle Ricerche, Istituto per le Risorse Biologiche e le Biotecnologie Marine (CNR-IRBIM), Italy

<sup>3</sup>Consiglio Nazionale delle Ricerche, Istituto di Scienze Polari (CNR-ISP), Italy

<sup>4</sup>NBFC, Centro Nazionale per la Biodiversità, Palermo, 90133, Italy

<sup>5</sup>FMC, Fano Marine Center, Italy

<sup>6</sup>Alma Mater Studiorum — Università di Bologna, Italy

<sup>7</sup>Seas Geosciences (Sealaska) Roma, Italy

Correspondence to: Irene Sammartino ([irene.sammartino@cnr.it](mailto:irene.sammartino@cnr.it))

**Abstract.** This study examines the sedimentary and microbial responses offshore the Marche Region (Italy) to the September 2022 flood, one of the most severe recent hydrological events, which delivered large amounts of sediment and anthropogenic contaminants to the Adriatic Sea. We employed a multidisciplinary approach integrating sedimentology, geochemistry, organic matter analysis, pollutant assessments (Polycyclic Aromatic Hydrocarbons, PAHs and Poly- and Perfluorinated alkyl substances, PFASs), and benthic microbial community structure. Sediments collected five days post-event offshore six river mouths reveal that flood deposits, ranging from fine sand to coarse silt, were largely confined within the nearshore zone down to the 15 m isobath. This distribution reflects intense riverine inputs and a brief windstorm-enhanced coastal circulation that generated patchy, temporary sediment accumulations in the prodelta sector. Heavy metal concentrations remained below regulatory thresholds, whereas organic pollutants were heterogeneously distributed, with peaks offshore urban and industrial zones. PAH signatures indicate mixed pyrogenic and petrogenic sources, while next-generation PFASs (6:2FTS) showed localized but severe contamination linked to upstream industrial activities. Simultaneously, the flood introduced strong spatial heterogeneity in benthic bacterial communities, with sediment texture and organic matter content driving compositional shifts. Freshwater-associated taxa became prominent in offshore deposits, highlighting riverine sedimentary imprints. Despite the flood's magnitude onshore, its offshore sedimentary and ecological signatures were spatially limited and ephemeral. These findings underscore the ecological significance of episodic sediment and contaminant inputs, while highlighting the challenges in detecting such transient events in the marine stratigraphic record.



## 35 1. INTRODUCTION

A warming climate is amplifying precipitation extremes (Allan and Soden, 2008; Nie et al., 2018; Fowler et al., 2021). Since 1950, annual precipitation maxima have risen at two-thirds of global weather stations, with record-breaking daily extremes becoming more common, especially since the 1980s (Westra et al., 2013; Lehmann et al., 2015; Merz et al., 2021; Sun et al., 2021; IPCC, 2023). Meanwhile, shifts in peak river discharge patterns worldwide (Do et al., 2017; Slater et al., 2021) underscore the growing influence of anthropogenic climate change on flood events (Kundzewicz et al., 2014; Blöschl et al., 2017; Syvitski et al., 2022). River floods rank among the most frequent and costly natural hazards (Winsemius et al., 2016; Kundzewicz et al., 2018). Their impact is expected to intensify due to rapid urbanization, soil loss and impermeabilization, and the consequent increasing extent of flood-prone areas (Dottori et al., 2023).

Small- to moderate-sized rivers ( $10^2$ – $10^5$  km<sup>3</sup>) play a crucial role in sediment dynamics and the formation of deposits on the shelf (Syvitski and Kettner, 2007; Pitarch et al., 2019; Pellegrini et al., 2021, 2024). While large rivers, such as the Amazon and Mississippi, drain most continental interiors (Vörösmarty et al., 2000), the number of small- to moderate-sized rivers directly discharging into coastal zones is orders of magnitude greater (Milliman and Syvitski, 1992; Syvitski et al., 2003; Cohen et al., 2022). In small watersheds, flood events are typically tightly coupled with the triggering storm, meaning that high river discharge often coincides with stormy sea conditions. In contrast, in large watersheds, river floods may reach the coast once the storm has passed, during calm marine conditions. This decoupling has important implications for the preservation (thickness, continuity and spatial redistribution) of river flood deposits offshore (Wheatcroft et al., 2006). Small rivers also exhibit more pronounced discharge fluctuations than large systems (Syvitski et al., 2003). For instance, Mediterranean rivers can experience peak discharges up to 40 times their base flow, whereas large rivers may see only a twofold increase during floods (e.g., Gomez et al., 1995). Given that suspended sediment concentration, and consequently sediment load, is a positive, non-linear function of fluid discharge (e.g. Gupta et al., 2021), frequent flooding of small rivers significantly influences sediment delivery to the sea (Pellegrini et al., 2021, 2024; Pierdomenico et al., 2022). In fact, the majority of sediment flux from small rivers likely occurs during short-lived (days to weeks) flood events (e.g., Blöschl, 2000; Wheatcroft and Drake, 2003; Winsemius et al., 2016; Merz et al., 2021), highlighting the critical role of floods in coastal sedimentation.



60 Event-response sampling has been instrumental in understanding the large-scale distribution, small-scale physical and chemical properties and formation mechanisms of multiple flood deposits on the continental shelf (Wheatcroft et al., 1997; Traykovski et al., 2000). The unpredictability of flood timing, which rarely aligns with ship scheduling, poses a major challenge for studying flood sedimentation. As a result, event-response sampling from small research vessels is essential (Wheatcroft, 2000; Trincardi et al., 2020; Pellegrini et al., 2023). In deltas, assessing the distribution of pollutant particles and the

65 development of microbial communities is particularly challenging, as accessing shallow-water, highly dynamic subaqueous environments immediately after a river flood event and in the tail of a storm remains practically difficult and challenging. In recent decades, significant efforts have been made to understand the key depositional processes shaping subaqueous coastal environments (e.g. Goodbred et al., 2003; Liu et al., 2006; Korus and Fielding, 2015; Vona et al., 2025). Sedimentation processes often impart distinctive, centimeter scale, structures to the resulting deposits. These structures reflect the complex

70 interplay between sediment supply and the physical and biological processes active at the time of deposition. As such, sedimentary structures provide crucial insights into depositional conditions and are widely used to interpret sediments, even within inner-shelf mud deposits (e.g., Nittrouer et al., 1986; Bentley & Nittrouer, 2003; Bhattacharya and MacEachern, 2009; Jaramillo et al., 2009; Macquaker et al., 2010; Ainsworth et al., 2011; Patruno and Helland-Hansen, 2018; Peng et al., 2022; Pellegrini et al., 2024). Inner-shelf mud deposits serve as important sites of organic carbon (OC) accumulation, contributing

75 substantially to global OC burial (Tesi et al., 2007; Sanchez-Vidal et al., 2013; Bao et al., 2016; Pellegrini et al., 2021). In addition to high sedimentation rates, OC preservation in these deposits is enhanced by the relatively low reactivity of land-derived material, which undergoes early diagenetic alteration and is matrix-protected against degradation (Mayer, 1994; Mead and Goñi, 2008). Furthermore, hypopycnal coastal plumes foster intense new primary productivity, adding another source of organic biomass accumulating at the seafloor along the shelf (Lohrenz et al., 1990; Campanelli et al., 2011; Vona et al., 2025).

80 Coastal systems are a temporary storage for river-borne sediments (e.g., Bao et al., 2016; Bianchi et al., 2018; Pellegrini et al., 2021, 2024) and can accumulate anthropogenic materials catchments (Simon-Sánchez et al., 2019; Lim et al., 2021; Pierdomenico et al., 2022; Pellegrini et al., 2023; Trincardi et al., 2023; Bolan et al., 2024; Iemeljanov et al., 2024; Weiss et al., 2024;; Adeoba et al., 2025; Bue et al., 2025; Gruca-Rokosz et al., 2025; Jalaosho et al., 2025; Nikki et al., 2025; Owowenu et al., 2025), especially in prodeltas, that are the delta sector lying beyond the delta front in a submerged environment where

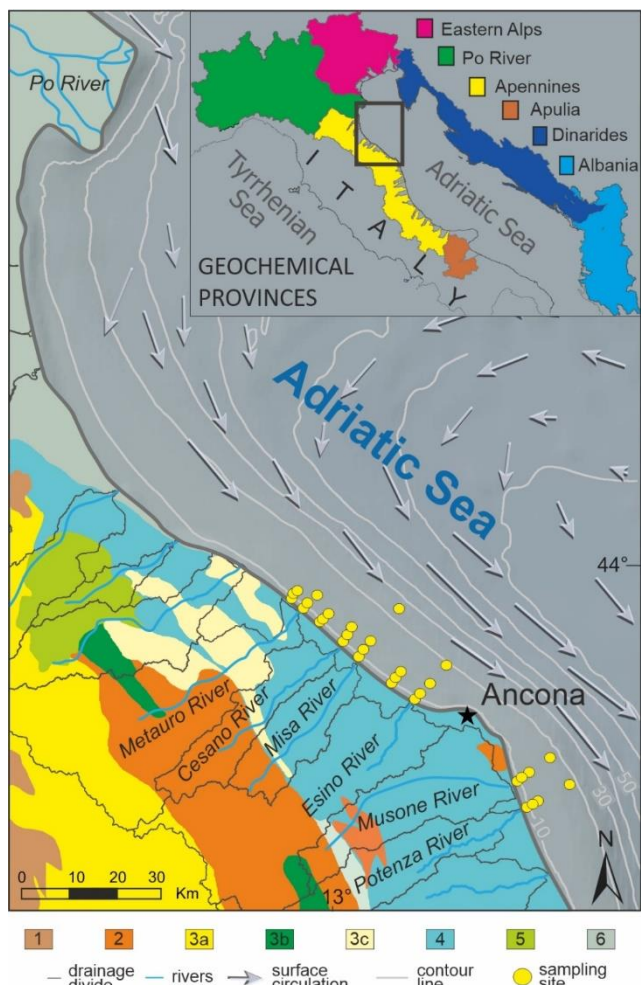


85 the highest sediment accumulation rate are reached (Coleman and Wright, 1975; Pellegrini et al., 2020). Riverine sediments play a fundamental role in the supply of hazardous metals and other contaminants to coastal areas, often reflecting significant sources of pollution (e.g. Lucchini et al., 2001; Sammartino, 2004; Amorosi and Sammartino, 2007; Jeon et al., 2011; Munoz et al., 2017; Amorosi et al., 2022; Riminucci et al., 2022; Fanelli et al., 2025; Frapiccini et al., 2024). Mineralogical composition, organic matter content, and textural characteristics of sediments represent valuable natural archives of recent environmental changes, acting as key carriers and repositories for harmful contaminants within aquatic ecosystems (Rath et al., 2009; Amorosi et al., 2014). Among coastal environments, river deltas are particularly dynamic, responding rapidly to both natural and anthropogenic changes (Syvitski et al., 2005, 2009; Blum and Roberts, 2009; Falcini et al., 2012; Bosman et al., 2020; Trincardi et al., 2020). These systems are subject to intense human pressures (Gardner et al., 2023; Haq and Milliman, 2023; Anthony et al., 2024), which modify river discharge, sediment supply, and coastal morphology (Vörösmarty et al., 2003; Overeem and Brakenridge, 2009; Hood, 2010; Anthony et al., 2014; IPCC, 2021; Syvitski et al., 2022; Warrick et al., 2024). Despite their importance, the impact of river flood deposits on the spatial distribution of organic and inorganic sediments, remains poorly understood as well as the mobilization, transport and bioavailability of contaminants, and their influence on microbial community development. This knowledge gap limits our ability to accurately assess the impact of river floods in transitional environments and design effective mitigation measures, especially in the context of climate change. Understanding the dynamics at the land-ocean interface is critically limited by the scarcity of data on short-lived, high-impact flood events. These episodic phenomena can drastically alter the spatial distribution of organic and inorganic sediment, influence the mobilization and bioavailability of contaminants, and reshape microbial community structure. Yet, their transient nature implies that these deposits remain elusive to conventional sampling strategies, typically decoupled from the timing of such events.

105 This study addresses this gap by studying the September 2022 flood in the Marche region (Fig. 1) as a rare observational opportunity. Samples were strategically collected from freshly deposited surface sediments and from underlying, pre-flood bottom deposits, allowing for a direct comparison to isolate the effects of the flood. By capturing sedimentary, geochemical, and biological signals shortly after the event, we provide novel insights into early deposition processes and spatial patterns triggered by floods. This event-focused approach highlights the added value of timely, targeted sampling in advancing our



110 understanding of pollutant dynamics, microbial responses, and organic carbon fate in transitional environments, ultimately



supporting more accurate predictive frameworks and effective mitigation strategies.

**Figure 1: Geological and hydrographic map of the central Adriatic region, highlighting major river basins in the Marche region (Metauro, Cesano, Misa, Esino, Musone, Potenza). Colors indicate main geological formations; gray lines mark drainage divides. Yellow dots show coastal sampling sites. Gray arrows represent surface circulation**

115 **(averaged measurements of drifter velocities; Poulain, 2001). Inset: geochemical provinces of northern and central Adriatic Sea as documented in Amorosi et al., 2022, with the study area outlined (black box) and major sediment provenance domains indicated.**



## 2. APPROACH

### 120 2.1 Study area and the 2022 flood event

The September 2022 rainfall event occurred after a prolonged period of drought, that has strongly affected the catchment, and lasted approximately twelve hours (Donnini et al., 2023; Pulvirenti et al., 2023). On September 15<sup>th</sup>, several thunderstorms affected the northern and central mountainous and high-hilly areas of the region, with rainfall decreasing in intensity while moving towards the coast. In the late afternoon, a self-regenerating and stationary system formed, eventually affecting also the hills and coastal areas. This system caused widespread critical conditions in the river basins (e.g., Cesano and Misa rivers; De Lucia et al., 2024) with cumulated rain values peaking up to 90 mm/h and 400 mm/6 h (data from Regione Marche, Centro Funzionale Regionale). As a consequence, river levels rose rapidly - by up to five meters in just three hours (Fig. 2) - with flood thresholds exceeded at multiple sites and widespread inundation reported. On the following day, a similar, yet weaker, thunderstorm system developed to the windward side of the Apennines, affecting additional catchments to the south (i.e., 130 Potenza River, see Fig. 2) with cumulated rain peaking up to 140 mm over the event. Finally, a development of a low-pressure system over the central Adriatic Sea on September 17<sup>th</sup> led to additional scattered showers and to a rapid intensification of winds from the north-east. Although this low-pressure system exited the region by the end of the day, the associated windstorm was influential on the fate of the sediment discharged by the flood to the coastal area.

### 135 2.2 The 2022 Rapid Response Cruise (RRC)

Surface sediment samples were collected on board the R/V *Tecnopesca II* on September 23<sup>rd</sup>, 2022, just five days after the major flooding event that impacted the central Adriatic coast. Sampling took place along nine coast-to-offshore transects, corresponding to six primary river mouths affected by the flood, as well as three intermediate transects (Fig. 1). The number of sampling stations extended offshore until flood-related deposits were no longer detectable. Sediment was retrieved from 140 each station using a 25 L Van Veen grab, which allowed the recovery of approximately 60 kg (25,000 cm<sup>3</sup> x 2.5 g cm<sup>-3</sup>) of sediment. The grab allowed for the sub-sampling of the sediment succession up to 25 cm in depth to examine the sedimentary expression of the 2022 flood event (Fig. 2). In addition, sub-samples of pre-flood deposits were collected to better characterize changes induced by the event. All sub-samples were labeled with the cruise acronym (RRC) and stored in sterilized glass vials.



Pollutants analyses were carried out on a subset of sediment samples. Specifically, two sampling points for each of the nine  
 145 analyzed transects were selected: the first one is located closer to the coast, the second one at the furthest point. For each of  
 these 18 sampling points, two aliquots of sediment were taken: the first one (top) corresponding to the 2022 river flood deposits,  
 the second one (bottom) referring to pre-flood sedimentary deposits.

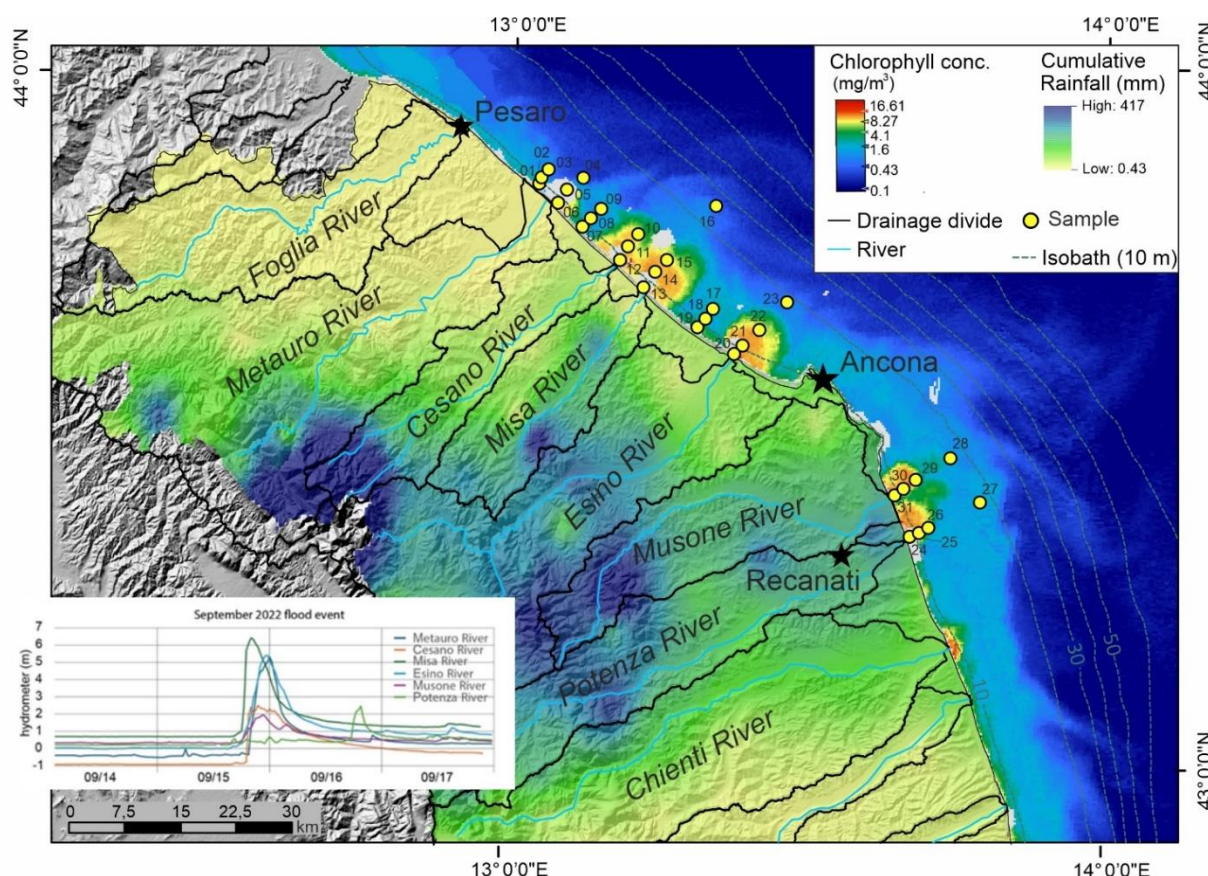


**Figure 2: Cumulative rainfall (in mm) recorded between 4:00 PM on September 15<sup>th</sup> and 1:00 AM on September 16<sup>th</sup>,  
 150 along with hydrometric levels measured at gauging stations located along major rivers affected by the September 2022  
 flood: Metauro River (Acqualagna), Cesano River (San Michele al Fiume), Misa River (Bettolle), Esino River  
 (Campononecchio), Musone River (Montepolesco), and Potenza River (San Severino Marche).**

### 3. DATA AND METHODS

#### 3.1 Sedimentological analyses on organic and inorganic particles



Sedimentological analyses were conducted at different resolutions from m to  $\mu\text{m}$ -nm scale. The stratigraphic description, coupled with high-resolution photographic images, was used to characterize subtle sedimentary structures in fine-grained sediments. A subset of samples, exhibiting noticeable changes in texture, was selected for Scanning Electron Microscope (SEM) analysis to identify sediment fabric and reconstruct the main sedimentary processes (Fig. 3). SEM samples were stabilized with Spurr resin after pore water was removed using acetone (Schimmelmann et al., 2015), and then ion-milled (Schieber, 2013). The same methodology was applied to analyze primary sedimentary structures and fabrics in Holocene Adriatic samples (Pellegrini et al., 2021, 2024). The milled sample surfaces were examined without a conductive coating using a FEI Quanta 400 FEG (Field Emission Gun) in low vacuum mode. Energy Dispersive X-ray Spectroscopy (EDS) was used to determine the composition of the sedimentary particles.

Granulometric analysis and water content determination were conducted on sediment aliquots from each sampling station for both the 2022 river flood and pre-flood deposits. Approximately one spoonful of wet sediment was weighed using an analytical balance with mass measurements to two decimal places. The sediments were then dried at  $50^{\circ}\text{C}$  for 24 hours, re-weighed, and the ratio of wet to dry sediment mass was calculated. Grain size was determined using a Malvern Mastersizer 3000 analyzer (Hydro EV), which covers size ranges from 0.01 to  $3500\ \mu\text{m}$ , at the Geohazard core laboratory of the Institute of Marine Science of the National Research Council (CNR-ISMAR), Bologna. Sediment samples were dispersed in demineralized water for 24 hours and subjected to ultrasonic treatment for 60 seconds prior to analysis. Laser-scattering spectra were processed using the Multiple Sample Statistics sheet in the GRADISTAT MS Excel worksheet (Blott and Pye, 2001). The grain-size analysis includes all particles in the sample and results are reported according to the Wentworth scale (Wentworth, 1922). Organic matter characterization was performed at both bulk and molecular levels. Sedimentary organic carbon was analyzed using stable carbon isotopes ( $\delta^{13}\text{C}$ ) via EA-IRMS (Elemental Analyzer-Isotope Ratio Mass Spectrometry), following the method outlined by Tesi et al. (2007). In brief, freeze-dried and ground samples were placed in silver capsules, acidified with 1.5 M HCl to remove the inorganic fraction, and analyzed using a Finnigan DeltaQ Mass Spectrometer, directly coupled to a Thermo Fisher Scientific FLASH 2000 IRMS Element Analyzer through a ConFlo IV interface for continuous flow measurements. The standard deviation, based on replicate analyses of the reference standard (IAEA-CH7) and in-house standards, was  $< \pm 0.1\%$ .



$\delta^{13}\text{C}$  data from recent studies on the supply and deposition of Terrigenous Organic Carbon ( $\text{OC}_{\text{Terr}}$ ) along the Adriatic coastal system were compiled to define the terrigenous end-member and provide context for the RRC2022 samples. Our dataset included Po River suspended sediments from the 2011 flood, river-bed sediments from the Apennine rivers (2005), and Po River flood deposits (2000-2009). All terrigenous samples displayed the depleted  $\delta^{13}\text{C}$  signature typical of land-derived material, with an average value of  $-26.46 \pm 0.44\text{‰}$  (Tesi et al., 2013; Pellegrini et al., 2021, 2024). The marine  $\delta^{13}\text{C}$  end-member ( $-20.4\text{‰}$ ) from Tesi et al. (2006) was used in the source-apportionment model.

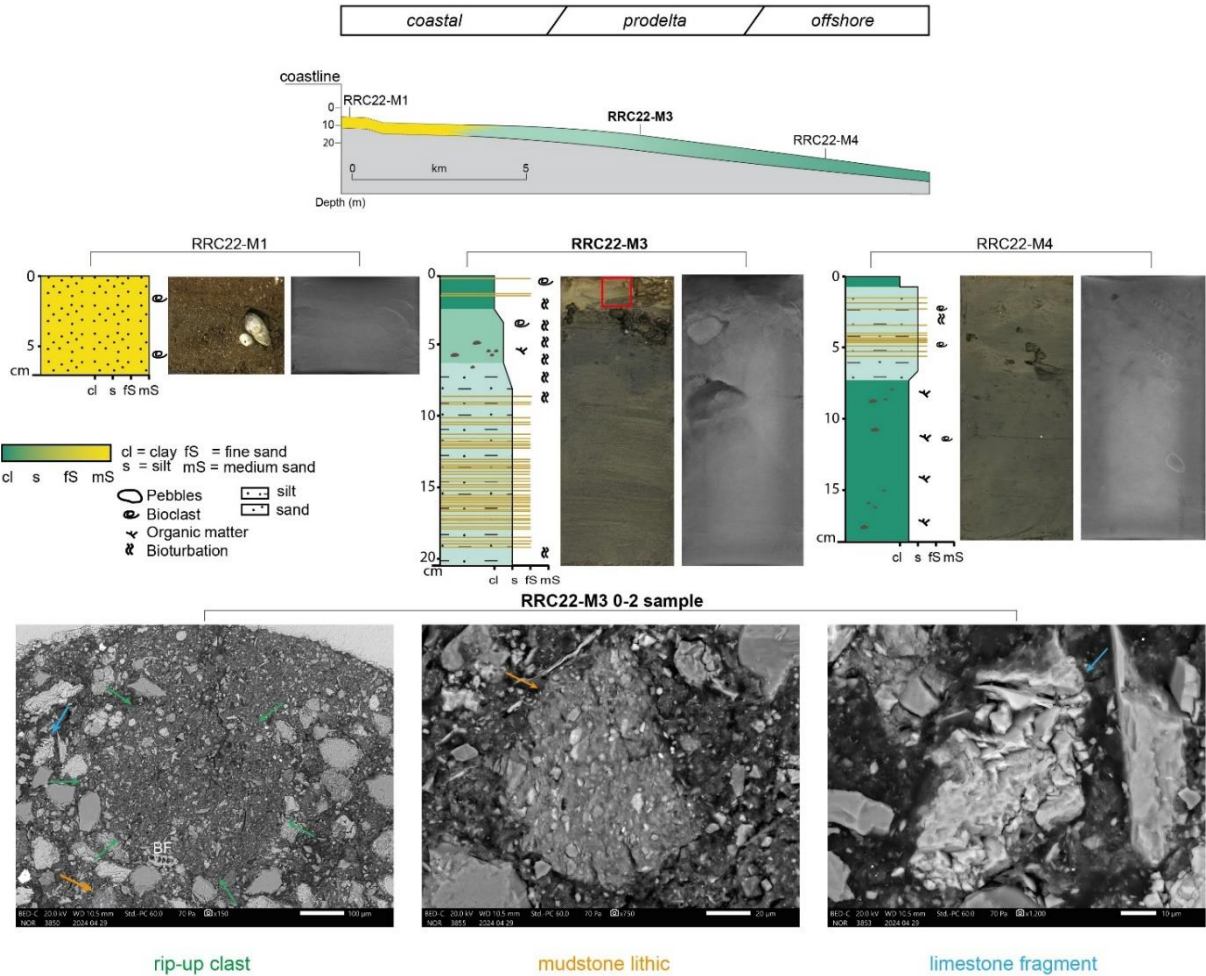


**Figure 3: The sedimentary expression of the 2022 river flood along a coast-to-sea transect offshore from the Misa River mouth: a) schematic section based on previously published seismic profiles (e.g., Cattaneo et al., 2003; Pellegrini et al., 2021); b) sedimentary logs illustrating the main lithological changes, sedimentary structures, bioclasts, and**



bioturbation features; and c) Scanning Electron Microscopy (SEM) images of ion-milled samples from sediment cores with fine-grained intraclasts, semi-consolidated rip-up clast (green arrow), mudstone lithic (orange arrow), limestone fragment (light blue arrow), benthic forams (BF).

### 195 3.2 X-Ray Fluorescence (XRF)

Geochemical analyses were performed to assess sediment provenance and hazardous metals content. Total concentrations of major and trace elements were determined using Wavelength-Dispersive X-Ray Fluorescence (WD-XRF). A total of 42 bulk sediment samples were analyzed at the University of Bologna. Samples were air-dried at 40°C and ground using an agate swing mill. The powders were then pressed into tablets and analyzed for major and trace elements using a Panalytical Axios spectrometer (Rh tube), applying matrix correction methods by Franzini et al. (1972, 1975), Leoni and Saitta (1976), and Leoni et al. (1986). Accuracy was verified through certified reference materials (Govindaraju, 1989), with uncertainties of 2% for Ni and Zn, 6% for Cu, 7% for Cr, and 10% for As and Pb.

To reconstruct sediment provenance, data were compared with geochemical analyses of riverine deposits from previous studies. Alpine and Apennine rivers provide distinct geochemical fingerprints reflecting their respective catchment geology (see Amorosi et al., 2022). The Po River basin drains the Western and Central Alps and the Ligurian-Emilian Apennines. The Western Alps are characterized by metamorphic and mafic-ultramafic (ophiolitic) rocks, while the Apennines consist mainly of shales, marls, and sandstones, with localized ophiolite exposures. This ultramafic imprint is evident in Po River sediments, which show elevated Cr and Ni concentrations (Fig. 1).

To assess sediment provenance, Ca-Al<sub>2</sub>O<sub>3</sub>, Cr-V and MgO-Ni/Al<sub>2</sub>O<sub>3</sub> diagrams were used as provenance indicators, plotting major and trace element composition of the study samples against sediment samples from the modern river network (Dinelli & Lucchini, 1999; Amorosi and Sammartino, 2007; Amorosi et al. 2022).

### 3.3 Polycyclic Aromatic Hydrocarbons (PAHs)

The PAHs analyzed in this study are those listed as priority pollutants by both the European Union and the US EPA. Sixteen compounds were targeted, including low molecular weight (LMW, 2-3 rings) PAHs: naphthalene, acenaphthylene,



acenaphthene, fluorene, phenanthrene, and anthracene, and high molecular weight (HMW,  $\geq 4$  rings) PAHs: fluoranthene, pyrene, benz[*a*]anthracene, chrysene, benzo[*b*]fluoranthene, benzo[*k*]fluoranthene, benzo[*a*]pyrene, dibenz[*a,h*]anthracene, benzo[*ghi*]perylene, and indeno[1,2,3-*cd*]pyrene. PAHs were extracted using a 50:50 dichloromethane/methanol solution in an ultrasonic bath (BRANSONIC 1510E-mt) for three 15-minute cycles. The extract was concentrated via rotary evaporation at 27°C and under nitrogen flow, then reconstituted in 0.4 mL of acetonitrile. Analyses were conducted via an UHPLC system (UltiMate 3000, Thermo Scientific), equipped with a Diode Array Detector (DAD) and a fluorescence detector (RF2000, Dionex). Instrumental details are reported in Frapiccini et al. (2024). Method validation followed ICH Q2B guidelines (ICH, 2005), using LOD = 3.3 Sa/b and LOQ = 10 Sa/b, where Sa is the standard deviation of the intercept and b is the calibration slope. Recoveries were verified using IAEA-408 and IAEA-383 reference materials. LODs, LOQs, and recovery rates are presented in Tables S1 and S2.

To investigate PAH sources, diagnostic ratios were used, distinguishing between petrogenic (originating from petroleum) and pyrogenic (from combustion) origins. Ratios calculated include: LMW/HMW, anthracene/(anthracene + phenanthrene),  $\Sigma\text{COMB}/\Sigma\text{PAHs}$ , fluoranthene/(fluoranthene + pyrene), and benz[*a*]anthracene/(benz[*a*]anthracene + chrysene) (Yunker et al., 2002; Arienzo et al., 2017; Maletić et al., 2019). Petrogenic PAHs are typically waterborne and deposited directly in sediments, while pyrogenic PAHs are airborne before entering aquatic systems.  $\Sigma\text{COMB}$  includes fluoranthene, pyrene, benz[*a*]anthracene, chrysene, benzo[*b*]fluoranthene, benzo[*k*]fluoranthene, benzo[*a*]pyrene, indeno[1,2,3-*cd*]pyrene, and benzo[*ghi*]perylene. A  $\Sigma\text{COMB}/\Sigma\text{PAHs}$  ratio  $> 0.8$  indicates a pyrogenic origin;  $< 0.8$  suggests a petrogenic one. Similarly, anthracene/(anthracene + phenanthrene)  $> 0.1$  and fluoranthene/(fluoranthene + pyrene)  $> 0.5$  both point to pyrogenic sources. Conversely, ratios below those thresholds suggest petrogenic origins. Lastly, benz[*a*]anthracene/(benz[*a*]anthracene + chrysene)  $> 0.35$  also implies pyrogenic input (Lee et al., 2021; Mali et al., 2022).

### 3.4 Poly- and Perfluorinated alkyl substances (PFASs)

The extraction of the analytes from the matrix was performed using an Accelerated Solvent Extractor (ASE™ 350, Thermo Fisher Scientific Dionex Inc.). About 10 g wet weight of fresh sediment samples were homogenized and mixed with diatomaceous earth (Applied Separations Inc.), anhydrous sodium sulfate, and activated metallic copper (Sigma-Aldrich Co.),



to remove humidity and elemental sulfur from samples, then placed in a 20 mL cell and spiked with a known amount of D and  $^{13}\text{C}$  isotope-labeled solution. The extractions were carried out at 100 bar and 100°C using methanol as extraction solvent. The extraction procedure, 5 minutes static after a 5-min equilibration time, was repeated three times. The extracts were collected together, evaporated at 30°C under a gentle nitrogen stream to 10 mL (Turbovap<sup>®</sup> II, Caliper Life Science Inc.), and then  
245 diluted with 25 mL of deionized water. Clean-up was performed by Solid Phase Extraction (SPE) using Oasis HLB cartridge (Waters Corp.; Hydrophilic-Lipophilic Balance, 500 mg, 6 mL, 60  $\mu\text{m}$ ) previously conditioned by passage of 10 mL of methanol, followed by 10 mL of deionized acidified water. The extracts were passed through the cartridges under a pressure of 0.3 bar. The cartridges were then washed with 10 mL of deionized acidified water to remove all the salts and dried by passage of air for 5 min. The analytes were eluted with 10 mL of methanol at a rate of one drop per second and the eluate was  
250 diluted 1:1 (v/v) with deionized water.

Instrumental analyses were performed using an Agilent 1100 Series HPLC Value System (Agilent Technologies Inc.), coupled with a triple quadrupole API 4000<sup>™</sup> LC-MS/MS System, equipped with an ESI Turbo V<sup>™</sup> source (Applied Biosystems/MDS SCIEX PTE. Ltd.), operating in negative polarity. Data acquisition was obtained in MRM (Multiple Reaction Monitoring) mode with a 50 ms dwell time/transition. We considered 17 analytes, belonging to both target and next-generation PFASs.  
255 Quantification was performed using internal standards and the isotopic dilution technique. Results were corrected using the instrumental response factors and subtracting the procedural blanks. All sediment concentrations were calculated on a dry weight (dw) basis (Tab. S3). The quality control of the entire analytical procedure, in terms of repeatability (expressed as relative standard deviation), trueness (expressed as relative error), and percentage of recovery, was performed on five replicates of a fortified real environmental matrices (sediments collected in the Venice Lagoon at a depth of 10 m, dated back to the  
260 Pleistocene age and for these reasons judged free from modern contaminant compounds (Pizzini et al., 2024), and in compliance with the US EPA 1663A method.

### 3.5 Microbial communities

DNA was extracted from superficial (uppermost 0-1 cm) sediment samples using the DNeasy PowerSoil Kit (Qiagen)  
265 following the protocol described by Basili et al. 2021. Extracted DNA was stored at -20°C until further analysis. Quantification



of DNA was followed by PCR amplification targeting the V4–V5 hypervariable region of the 16S rRNA gene using the primer pair 518F-926R. PCR products were purified and indexed libraries prepared using the Nextera library preparation protocol and sequenced on the Illumina NextSeq2000 platform using a  $2 \times 300$  bp paired-end protocol. Raw sequence data were processed using Cutadapt (Martin, 2011) to remove primer and adapter sequences. Paired-end reads were imported and analyzed in RStudio (version 4.4.0) with the DADA2 package (version 1.32) (Callahan BJ, et al. 2016). Quality filtering was performed according to DADA2 guidelines, using maximum allowable estimated errors of  $>2$  and 2 per read for forward and reverse reads, respectively. Reads were merged into amplicon sequence variants (ASVs) based on 100% sequence identity. Chimeric sequences were identified and removed. Taxonomic classification was conducted using a naive Bayesian classifier against the SILVA database (version 138). Chloroplast and eukaryotic sequences were excluded from the dataset, and samples with low ASV counts were omitted (Table S2). Abundance values were normalized using the median of the dataset with the vegan (version 6.1) (Oksanen et al., 2025) and phyloseq (version 1.48) (McMurdie and Holmes, 2013) R packages and subsequently converted to relative abundances for further analyses. Raw sequence files are freely available in the Sequence Read Archive (NCBI SRA, <https://www.ncbi.nlm.nih.gov/sra/>), accession PRJNA1280684.

### 280 3.6 Meteorological and Oceanographical datasets

Atmospheric fields are provided by the Numerical weather prediction model MOLOCH, developed and implemented at the Institute of Atmospheric Sciences and Climate of the National Research Council (CNR-ISAC). MOLOCH is a non-hydrostatic, fully compressible, convection-permitting model, implemented with a horizontal resolution of 1.25 km. The operational chain produces daily 48h-forecasts with hourly resolution (<http://www.isac.cnr.it/dinamica/projects/forecasts>). Further details on the model can be found, e.g., in Davolio et al. (2017).

Oceanographic and sea state model data are provided by the ADRIAC operational system (Bressan et al., 2017), maintained by the Emilia-Romagna Regional Environmental Protection Agency (ARPAE). The system provides daily 72 hours forecast with hourly resolution and horizontal resolution of 1 km. The system is an implementation of the coupled model COAWST (Warner et al., 2010) over the Adriatic Sea, in particular with the ocean (ROMS) model and the wave (SWAN)





290 model coupled two-way forced by the atmospheric model ICON. Forecast output are open and accessible at <https://dati-simc.arpa.e.it/opendata/adriac/>.

In addition to model data, sea state and ocean currents observations have been collected at the marine weather station TeleSenigallia (see, e.g., Ravaioli et al., 2016), located near Senigallia (Ancona) 1 nm offshore at 12.5 m depth, equipped with an upward looking bottom mounted Teledyne Workhorse sentinel 300 KHz ADCP and maintained by the Institute for Marine  
295 Biological Resources and Biotechnology of the National Research Council (CNR-IRBIM), and at the ANCONA wave buoy, part of the Italian National Wave Buoy Network, courtesy of Italian Institute for Environmental Protection and Research (ISPRA, <https://www.isprambiente.gov.it/en>).

### 3.7 Statistical analyses

300 Statistical analyses were performed in Rstudio Alpha diversity, represented as ASV richness, was calculated using the vegan package. Differences in richness values across sample types were evaluated using an ANOVA test (stats package, version 4.4.0), incorporating data from all transects. Post-hoc pairwise comparisons were performed using Tukey's HSD test to identify specific group differences. Beta diversity was assessed using non-metric multidimensional scaling (NMDS), comparing samples from different transects and examining variations based on their distance from the coast, using PERMANOVA  
305 analysis. To identify microbial biomarkers associated with river flood impact, a Linear Discriminant Analysis Effect Size (LEfSe) was performed. Finally, taxa associated with freshwater discharge were also identified as described in Massaccesi et al. (2025).

## 4. RESULTS

### 310 4.1 Spatial distribution of inorganic and organic components of sediments

Grain size analyses reveal a slight decreasing trend in particle size in the 2022 river flood deposit, distinctive from older deposits. Additionally, a progressive decrease in particle size is observed along all coast-normal transects (Fig. 4). Fine sand to coarse silt is primarily confined near the coastline and in less than 10 m water depth (Fig. 4), where sedimentary structures with oblique- and cross-lamination are present (Fig. 3). In contrast, further offshore muddy beds show an irregular surface at



base and an overall fining up deposit (Figs. 3 and 4). The flood deposit shows relatively high bioturbation, few rounded pebbles, clasts and bioclasts content (Fig. 3). SEM imaging shows slightly sorted mudstone matrix with semi-consolidated clasts, detrital carbonate debris, and muscovite flakes (Fig. 3). Mudstone lithics can contain pyrite grains that likely were oxidized through outcrop weathering; limestone fragments are abundant (Fig. 3). Metal distribution in the flood sediment, reported in box and plots diagrams, shows concentrations much lower than the Italian permissible limits (Fig. 5). The flood deposits thin progressively seaward and are not present beyond the 15 m isobath (Figs. 3 and 4). Total Organic Carbon (TOC) increases by up to one order of magnitude in seaward sectors, reaching up to 1.2% (Fig. 4). Concurrently,  $\delta^{13}\text{C}$  data indicate relatively higher  $\text{OC}_{\text{Terr}}$  concentrations, especially seaward of the Misa and Esino rivers (Fig. 4). Notably, fine sand laminations are observed only in sediments deposited prior to the 2022 event (Fig. 3). These earlier sediments exhibit lower TOC content and more depleted  $\delta^{13}\text{C}$  values (Fig. 4). For all elements, pre-flood sediments record values slightly lower than the flood. Only two samples, 04 (Metauro3) and 05 (Metauro2) from the Metauro River transect, revealed two outliers (values exceeding 1.5 times the interquartile range) for Cu, with concentrations of 50 and 56  $\text{mg kg}^{-1}$ , respectively, however well below the threshold limit of 120  $\text{mg kg}^{-1}$ . (Fig. 5).

As shown by the scatterplot diagrams (Fig. 6), sediment supplied from the Po River show high chromium and nickel concentrations, whereas relatively high calcium content typifies the Apennine provenance. Consistent with their geographic location close to the fluvial mouths of Apennine rivers, almost all samples plot in the field of Apennine composition, with the sole exception of sample 16 (collected >15 km from the coast), which is characterized by lower Ca and higher Cr concentrations and likely reflects Po River influence via the longshore currents. In general, there is strong overlap in composition between flood and pre-flood samples (Fig. 5), suggesting continuous supply from the Apennine rivers, regardless of the competence of individual flood events (Fig. 6).

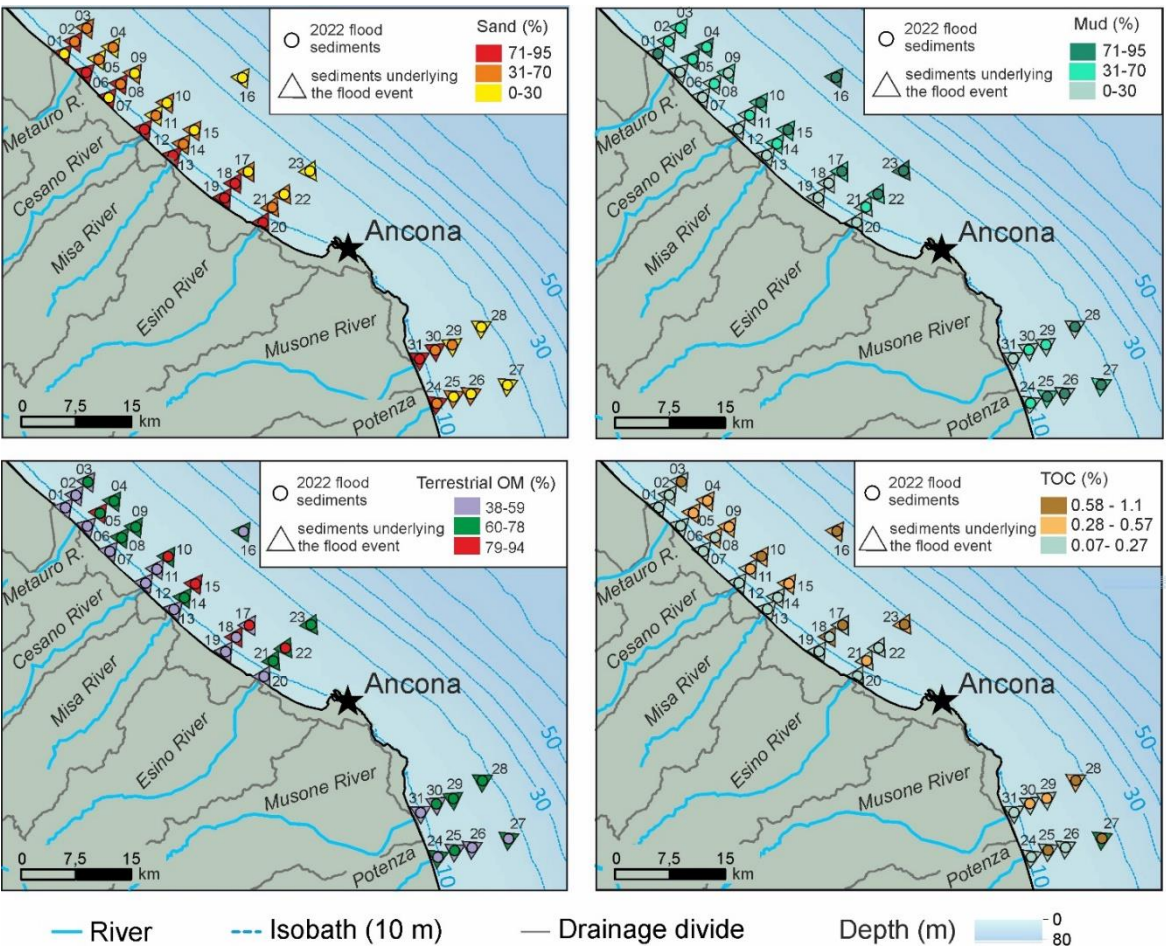


**Figure 4: Sediment properties and geochemical parameters in the coastal, prodelta and offshore area of Marche region.** Maps show distributions of sand (%), mud (%),  $\delta^{13}\text{C}$  (‰), and total organic carbon (TOC, %) at sampling stations. Colored circles represent measured values for both samples of the river flood sediments deposited in 2022 (small circles) and in older underlying sediments (large circles); background shading indicates satellite-derived chlorophyll-a concentration ( $\text{mg m}^{-3}$ ) as a proxy for surface productivity. Dashed lines are 10 m isobaths; rivers and drainage divides are also shown.

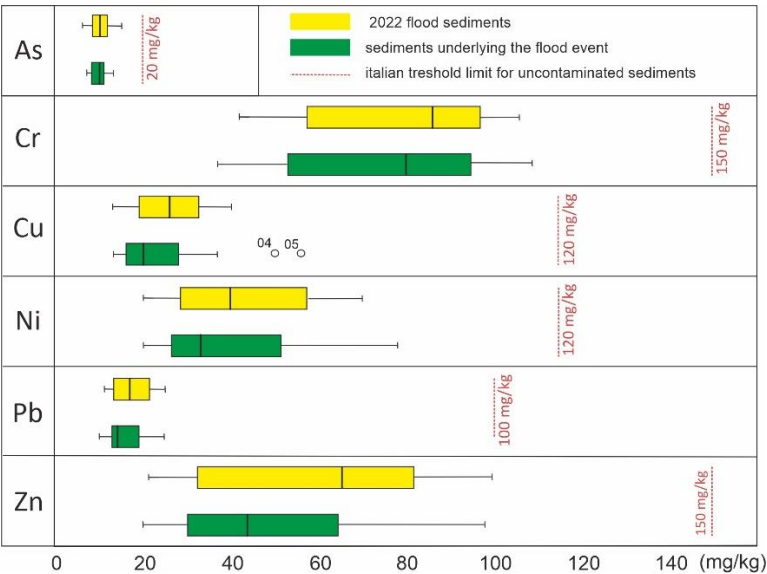


**Figure 5: Boxplots of metal concentrations (mg kg<sup>-1</sup>) in river flood sediments deposited in 2022 (Top) and in older underlying sediments (Bottom) for As, Cr, Cu, Ni, Pb, and Zn. Yellow and green boxes represent top and bottom sediments, respectively. Dashed red lines indicate sediment quality guideline thresholds. Outliers are shown as open circles.**

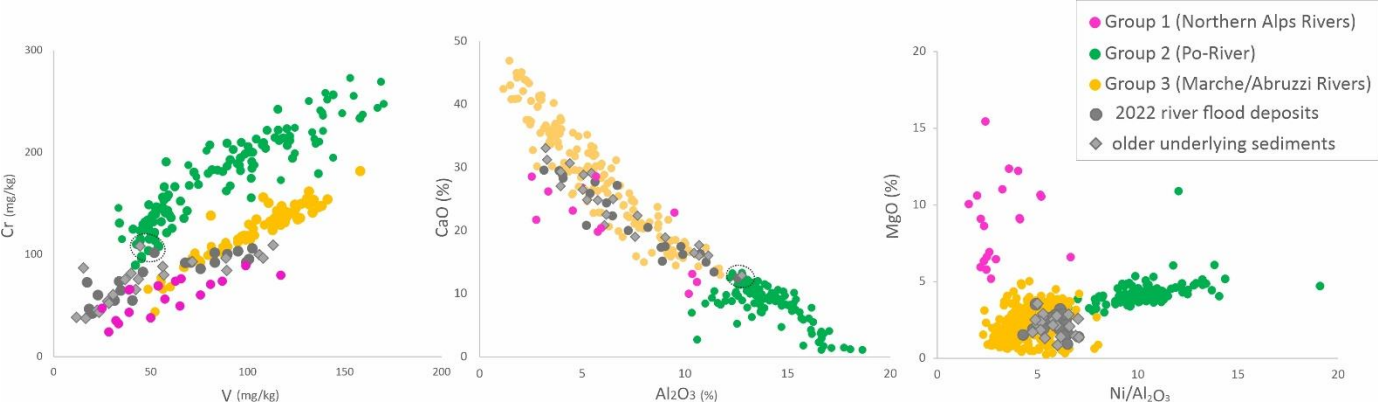


**Figure 6: Scatterplot diagrams of selected geochemical indicators of sediment provenance (Amorosi and Sammartino, 2007; Amorosi et al., 2022). Sediment from the Eastern Alps (Group 1) exhibits high CaO and MgO values, along with low Cr and Ni/Al<sub>2</sub>O<sub>3</sub>. Sediment from the Po River (Group 2) has low CaO and high Cr and Ni/Al<sub>2</sub>O<sub>3</sub>. Sediment from Marche/Abruzzi Apennines (Group 3) shows high CaO and low Cr, Ni/Al<sub>2</sub>O<sub>3</sub> and MgO. Samples analyzed in this study**



are consistent with an Apennine origin of the sediment from the Marche/Abruzzi catchments except for samples from site 16 (dashed line) which can be related to a mixed Apennine-Po River provenance.

#### 355 4.2 Polycyclic Aromatic Hydrocarbons

Total PAH concentrations differed between the various sampling sites, with the highest values found at the site sampled offshore of the Misa River (Misa3, 141 ng g<sup>-1</sup> dw), the river most affected by the flood event in the Marche Region, and lower values at the sampling site offshore of the Potenza River (Potenza 3, 15 ng g<sup>-1</sup> dw), less impacted by the flood event. In general, a consistent trend is observed across the sampled transects, with higher values at offshore sites compared to coastal ones (Fig. 7). The most common PAHs at coastal sites are acenaphthylene and fluoranthene, while the most common PAHs at the offshore sites are a cenaphthylene and phenanthrene. In all sediment samples analyzed, HMW PAHs were below 5 ng g<sup>-1</sup> dw (Fig. 7). Statistically significant differences (Mann-Whitman,  $p > 0.05$ ) between coastal and offshore samples were recorded for all individual PAHs, except for naphthalene, a cenaphthene, fluorene, and fluoranthene. Notably, the Misa River transect showed the largest difference between the offshore site (141 ng g<sup>-1</sup> dw) and the coastal site (25 ng g<sup>-1</sup> dw). Higher values in the open sea compared to the coastal one were also observed in the Cesano (69 vs. 27 ng g<sup>-1</sup> dw) and Metauro (50 vs. 18 ng g<sup>-1</sup> dw) river transects. A discrepancy in this pattern was observed in the Potenza River transect, where the values at the offshore site were lower than those at the coastal site (15 vs. 43 ng g<sup>-1</sup> dw). Some transects showed no significant difference between offshore and coastal sites, such as the transects at station A (52 vs. 47 ng g<sup>-1</sup> dw) and station C (30 vs. 31 ng g<sup>-1</sup> dw). The concentrations of total PAHs (ng g<sup>-1</sup> dw) in surface sediment samples, both offshore and coastal, are shown in Table S1. Figure S1 shows the percentage contribution of each individual PAH to their total amount. In most of the marine sediment analyzed, LMW compounds dominate, accounting for over 50% of the total PAHs. An exception is the sediment sample collected near the mouth of the Potenza River (Potenza 1), where the predominant PAH is fluoranthene, a four-ring aromatic compound considered HMW, which accounts for more than 40% of the total PAHs.

Investigated PAH isomer indicators such as  $\text{anthracene}/(\text{anthracene} + \text{phenanthrene})$ ,  $\text{fluoranthene}/(\text{fluoranthene} + \text{pyrene})$  and  $\text{benz(a)anthracene}/(\text{benz(a)anthracene} + \text{chrysene})$  show that the dominant sources of the investigated PAHs were primarily combustion-related (Fig. 8). Samples close to the coast, Potenza 1 and, in smaller amounts, Cesano 1 and C1 sites,





show a strong dominance of PAHs with pyrogenic sources. In all other cases,  $LMW/HMW$  and  $\Sigma COMB/\Sigma PAHs$  ratios also indicated a petrogenic sources for all samples, particularly in the sediments collected north of the flood event, and far from the coast (A1, Metauro3 and B3). Otherwise, Potenza1 site confirmed its pyrolytic origine. Particularly, A3 and Musone3 sites were more closely related to a petrogenic origin than a pyrogenic one (Fig. 8).

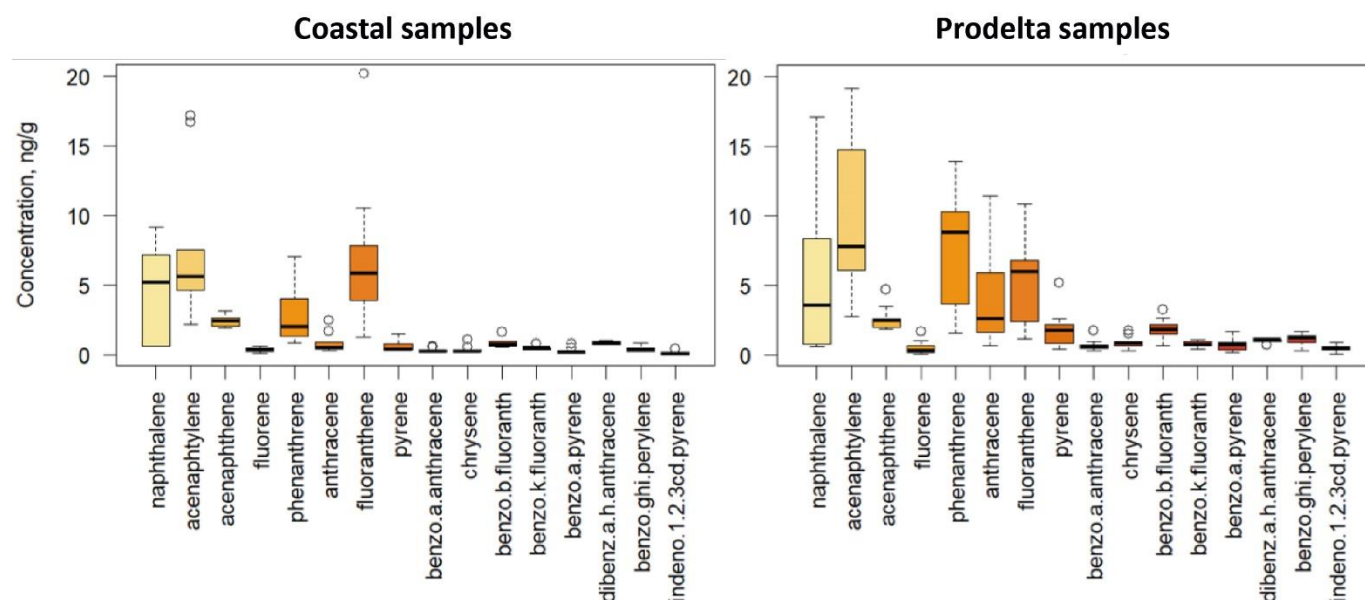


**Figure 7: Concentrations (ng g<sup>-1</sup> dry weight) of main PAHs in the 2022 river flood sediments. Boxplots show the distribution of individual PAH compounds, highlighting differences in composition and levels between nearshore and prodelta sectors. Outliers are shown as open circles.**

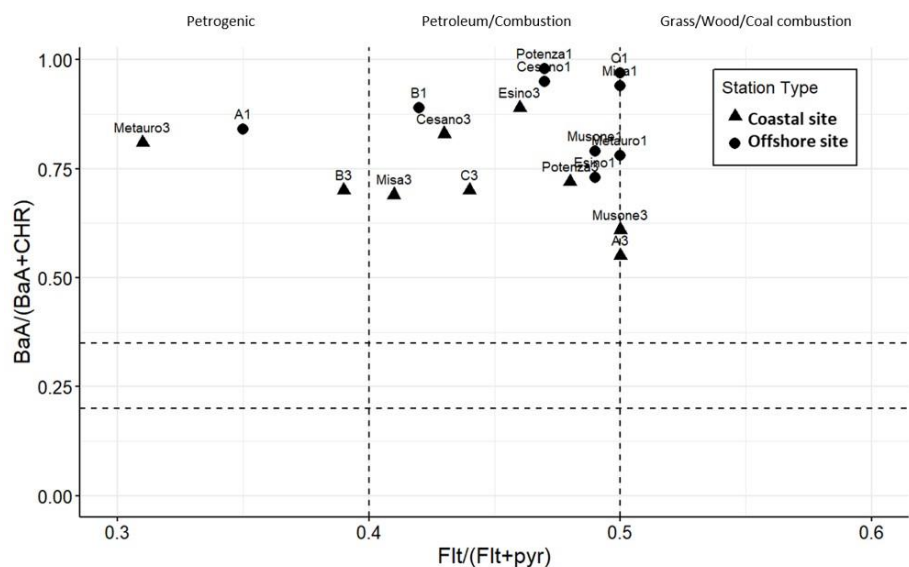


**Figure 8: Diagnostic ratio plot of PAHs using Flt/(Flt+Pyr) vs. BaA/(BaA+Chr) to infer the origin of organic matter in the 2022 river flood sediments. Coastal sites (triangle) and prodelta sites (circle) are classified into petrogenic, petroleum/combustion, and biomass/coal combustion sources based on threshold values (dashed lines) from literature.**

#### 4.3 Poly- and Perfluorinated alkyl substances

Among the 17 investigated PFASs, only six compounds were detected in the sediment samples: four belonging to the traditional target group and two fluorotelomer classified as next-generation PFASs. All other PFASs were below the Method Quantification Limits (MQLs; Fig. 9). Furthermore, a large proportion of the samples corresponding to the deeper, pre-flood sediment layers, showed no detectable PFAS contamination. Considering sediments deposited during the 2022 river flood, 6:2FTS remained the predominant compound, followed by an 8:2FTS contamination of lesser extent. These sulfonated fluorotelomers are considered next-generation PFASs, commonly used as replacements for legacy compounds due to regulatory restrictions, and are known for their high environmental persistence (Field and Seow, 2017). 6:2FTS was detected at consistently higher concentrations than those in the corresponding pre-flood layers (approximately two orders of magnitude greater), with values ranging from 0.203 to 86.10 ng g<sup>-1</sup> dw. This compound was detected both offshore and nearshore, with a general decreasing trend observed along almost all coastal-to-offshore transects. 8:2 FTS was also detected in the surface

sediments, though at lower concentrations ( $0.210\text{--}0.439\text{ ng g}^{-1}\text{ dw}$ ), and only in transects A (offshore), Metauro River and B (both sampling points), and in the nearshore sampling point of the Misa River transect (Fig. 9).

Perfluorohexanoic acid (PFHxA), perfluorooctanoic acid (PFOA), and perfluoroundecanoic acid (PFUnA) were each detected only in one sample, collected from the seaward sector of the Metauro River transect, at concentrations of  $0.120$ ,  $0.127$ , and  $0.208\text{ ng g}^{-1}\text{ dw}$ , respectively. Perfluorooctanesulfonic acid (PFOS), the only perfluorinated sulfonic acid (PFSA) identified, was detected exclusively in the seaward sector of the Esino River transect at a concentration of  $0.052\text{ ng g}^{-1}\text{ dw}$ , suggesting a very limited distribution of this compound across the study area. No PFASs were detected in transects associated to the Musone and Potenza rivers, both located South of the Ancona Promontory (Fig. 9).

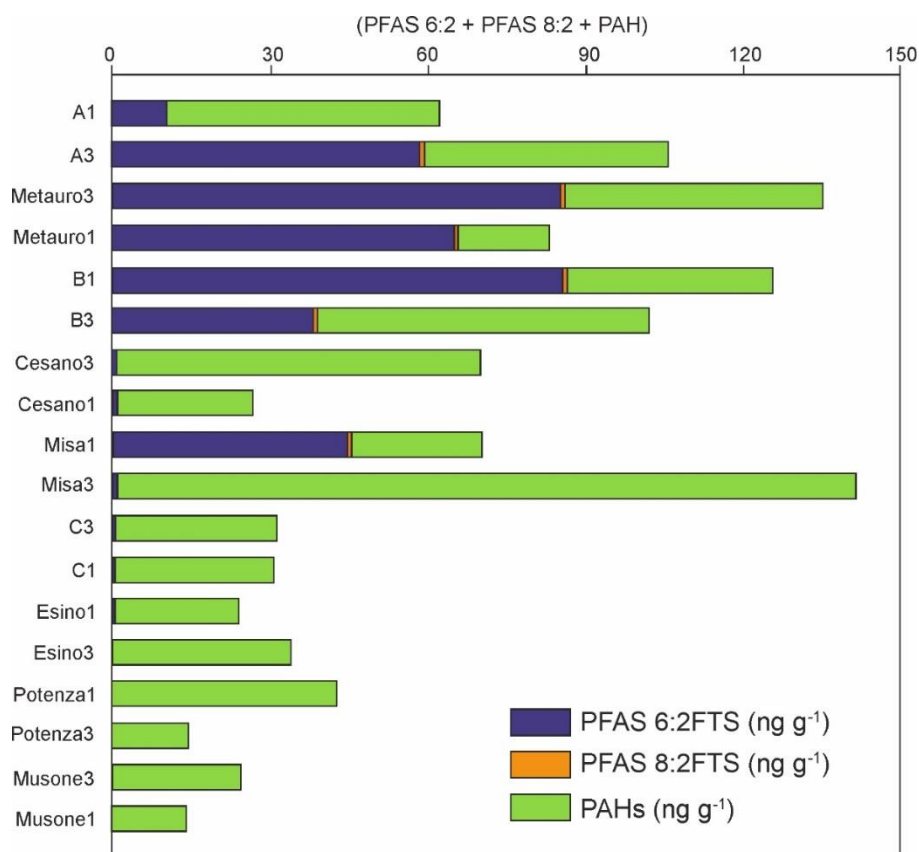


**Figure 9: Stacked bar chart showing the relative abundance of 6:2 FTS, 8:2 FTS (PFASs), and total polycyclic aromatic hydrocarbons (tot. PHAs) across all sampling locations.**



#### 4.4 Microbial communities' description

Microbial diversity increased progressively with distance from shore. Statistical analyses revealed significantly lower Shannon  
 415 diversity values in samples collected closer to the coast (ANOVA,  $p < 0.01$ ), particularly compared to offshore samples  
 (Tukey's test  $p < 0.01$ ). A similar, though not statistically significant, trend was observed for richness values (Fig. 10A).  
 Beta diversity analyses (Fig. 10B) revealed a clear spatial gradient in benthic prokaryotic community structure along the coast-  
 to-offshore transects (ANOSIM  $p = 0.001$ ,  $R = 0.6$ ), largely reflecting variations in sediment grain size, with the exception of  
 samples from the Musone River. Offshore samples formed a distinct cluster further composed by two subgroups, one  
 420 associated with silt and one with clay, TOC and TN (Fig. 10B).

All samples were dominated by Gammaproteobacteria (average  $26.39 \pm 2.61\%$ ), Bacteroidia ( $10.14 \pm 3.35\%$ ),  
 Thermoanaerobaculia ( $7.49 \pm 2.42\%$ ), and Planctomycetes ( $7.02 \pm 1.41\%$ ), with noticeable variability observed in their relative  
 abundances from coastal to offshore sites (Fig. S2).

LEfSe analysis (Fig. 10C) was conducted to identify microbial taxa significantly associated with sample groups defined by  
 425 their distance from the coast and flood impact. Coastal samples were significantly ( $p < 0.001$ ) enriched in  
 Thermoanaerobaculaceae, Pirellulaceae, and Woeseiaceae (genus *Woesia*), whereas prodelta samples were characterized by  
 the Desulfobulbaceae. Offshore samples displayed a higher relative abundance of Vicinamibacteria, Flavobacteriaceae and  
 Cyclobacteriaceae (Fig. 10C).

As an additional analysis to trace riverine influence, freshwater-indicator taxa were searched in the analysed samples. Results  
 430 showed that these taxa (i.e. Flavobacterium, Variovorax) were retrieved in offshore samples associated with clay, TOC and  
 TN (Supplementary Fig. S3), whereas they were largely absent or rare in coastal and silt-associated offshore sites.

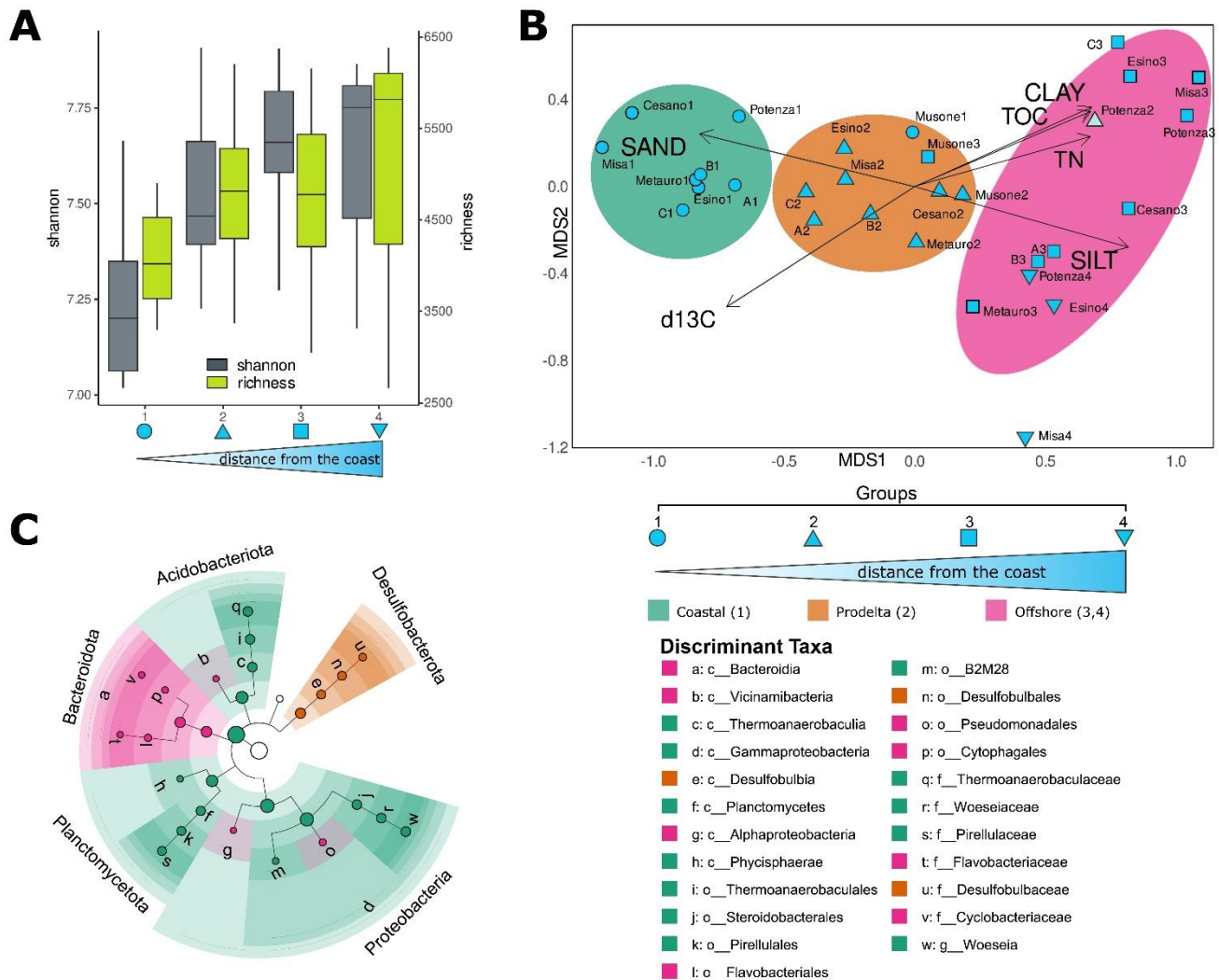


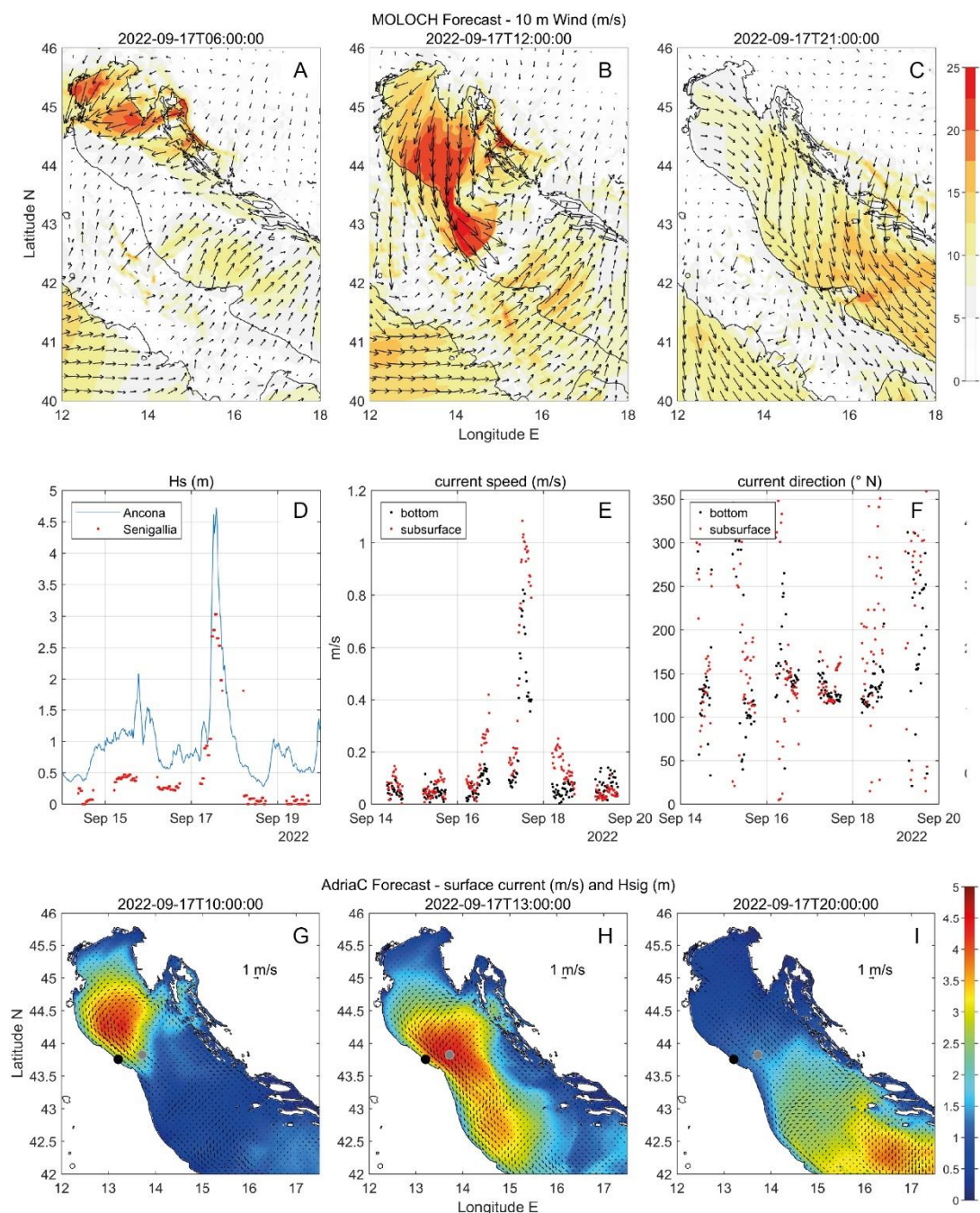
**Figure 10: Microbial community structure and diversity across the coastal-sea transect of the 2022 river flood sediments. Box plots of Shannon diversity and ASV richness (A) indices, clustered**  
by distance from the coast and river impact. (B) Non-metric Multidimensional Scaling (nMDS) ordination based on a  
Bray-Curtis dissimilarity matrix (Stress = 0.20); shapes indicate distance clusters, and ellipses represent 95%  
confidence intervals. (C) LefSe cladogram showing differentially abundant taxa ( $p < 0.001$ ) among clusters from the  
nMDS; each dot represents a discriminant taxon, colored by the cluster in which it is most abundant.





440 4.5 *Meteo-ocean conditions*

Oceanographic conditions along the coast during the flooding event were quite calm. This is true until September 17<sup>th</sup>, when a low-pressure system rapidly moving across the Adriatic Sea resulted (locally along the coast of the Marche Region) in gale-force northeasterlies during the afternoon, rapidly vanishing a few hours later. The evolution can be followed on Figure 11, showing the onset of northeasterlies in the early morning (Fig. 11a), directly impacting the coast at noon (Fig. 11b), finally  
445 rotating as northwesterly in the evening (Fig. 11c). Data collected offshore Senigallia and in Ancona show a rapid intensification of the sea state (Fig. 11d) with significant wave height of, respectively, 3 and 4.5 m, with a marked peak and rapidly decreasing later on. Data from the TeleSenigallia ADCP also show intensification of a longshore (ca. 120°, i.e., toward south-east, see Fig. 11f) currents with peak during the windstorm of 1 m s<sup>-1</sup> at the surface and 0.7 m s<sup>-1</sup> near bottom (Fig. 11e). As for the sea state, current intensity dropped quickly after a few hours. Ocean model data (Fig. 11g, h, i) provide a larger  
450 picture with the same features: rough sea state and accelerated coastal current at noon rapidly leaving the area toward the southern Adriatic following the disturbances. After a few hours, the Marche Region coastline turned back to calm sea state conditions and weakened coastal current. Although this windstorm did not last long, it followed closely the flooding event. Thus, it is relevant to take this into consideration while understanding the sediment transport right after the discharge.



455 **Figure 11: 10 m wind ( $\text{m s}^{-1}$ ) MOLOCH forecast valid time 17 September 2022 (A) 06:00 UTC, (B) 12:00 UTC, and (C) 21:00 UTC; (D) significant wave height (m) measured at Ancona (blue line) and Telesenigallia (red dots), (E) ocean currents speed ( $\text{m s}^{-1}$ ) measured by TeleSenigallia ADCP, along with (F) currents direction (degree, 0 N, flowing**



toward); ADCIRC forecast for significant wave height (m, color coded) and surface currents (black arrows) valid time  
 17 September (G) 10:00 UTC, (H) 13:00 UTC, (I) 20:00 UTC. The black filled circle indicates TeleSenigallia marine  
 460 station position. The gray filled circle indicates Ancona wave buoy position.

## 5. DISCUSSIONS

### 5.1 The ephemeral nature of river flood deposits

The sedimentary signature of river floods changes markedly with distance from the shoreline. In very shallow areas adjacent  
 465 to river mouths (approximately 5 m water depth), flood-related deposits are more difficult to identify. These nearshore sectors  
 are dominated by sandy sediment and subjected to remolding through high-energy processes including hyperpycnal flow  
 bypassing, wave-induced resuspension, and alongshore transport by coastal currents (Pailinkas & Nittrouer, 2006; Cattaneo et  
 al., 2007; Puig et al., 2007; Traykovski et al., 2007; Pellegrini et al., 2021, 2024). Additionally, coastal storm waves generate  
 bed shear stresses sufficient to erode and remobilize fine-grained sediment (Fain et al., 2007; Friedrichs & Scully, 2007;  
 470 Traykovski et al., 2007; Pellegrini et al., 2021, 2024). These conditions facilitated the bypass of riverine plumes from Apennine  
 catchments during the 2022 flood and limited the deposition of flood-derived sediment in the nearshore zone (Fig. 12).  
 In contrast, more distal prodelta environments (10–15 m water depth) offer a more favorable setting for the preservation of  
 flood deposits (Fig. 12). Here, sedimentary features such as rip-up clasts of semi-consolidated mud indicate erosion of  
 previously deposited fine-grained sediments. These characteristics are consistent with depositional patterns previously  
 475 described for the Pescara River prodelta (Pellegrini et al., 2024). The 2022 flood layers also exhibit a distinct  $\delta^{13}\text{C}$  signature  
 indicative of terrestrial origin (Tesi et al., 2007; Bao et al., 2016; Broder et al., 2018; Hage et al., 2022; Pellegrini et al., 2021;  
 Nogarotto et al., 2023), along with elevated concentrations of anthropogenic pollutants (Frapiccini et al., 2024; Fig. 12). The  
 PAHs concentrated in the prodelta sector, suggesting that such hydrophobic organic contaminants reflect the transport dynamic  
 of organic-rich riverine clays, following a similar dispersal pathway, as suggested also in other prodelta systems (e.g. Roussiez  
 480 et al., 2006; Bouloubassi et al., 2012). It is also important to highlight that in a few cases the PAH content in the Adriatic  
 prodelta deposits is five times higher than the nearshore samples (e.g. Misa River), highlighting the role of river flood in  
 creating focused pollutant hotspots (Fig. 12). Such considerations are of great concern from the environmental and ecological



viewpoints because coastal ecosystems are directly exposed to sediment-bound contaminants, which, with increasing extreme events, particle delivery will be enhanced during extreme hydro-meteorological events such leading to river floods.

485 Despite the severe damage and well-documented hydrological impact of the September 2022 flood event on land, its offshore sedimentary expression proved ephemeral. Our data show that flood-related deposits were largely confined to the nearshore zone, within the 15 m isobath, and in many cases were spatially discontinuous and patchily preserved. This limited offshore signature can be attributed to the interplay between concurrent high river discharge and high-energy meteo-marine conditions (Fig. 11). We hypothesize that reduced wave-induced shear stress in the prodelta sector allows for the partial settling of

490 suspended particles, while alongshore currents advect the sediment plume to the south, preventing offshore diffusion (Fig. 12). Similar sediment transport has been documented from satellite observations (Benincasa et al., 2019; Vona et al., 2025). While northeasterlies (Bora winds, see e.g., Signell et al., 2010) have relatively short fetch blowing perpendicular to the Adriatic Sea major axis, they can be severe enough to generate energetic waves (Pomaro et al. 2017). It is also well established that Bora windstorms in the Adriatic Sea enhance the Western Adriatic Coastal Current (WACC; e.g., Book et al. 2007) leading to

495 a alongshore sediment transport (Wang & Pinardi, 2002; Sherwood et al., 2004; Palinkas et al., 2007; Harris et al., 2008; Benincasa et al., 2019). During the 2022 event, the windstorm of September 17<sup>th</sup> was strong enough to produce offshore surface waves more than 4 m in significant wave height (Fig. 11d) and relatively long peak period (9 s, not shown), thus with significant impact on sediment remobilization when approaching the coast (Fig. 12). The rapid invigoration of the coastal current (Fig. 11e) intensified bed shear stress and alongshore transport. The relatively short duration of the windstorm limited the southward

500 displacement of sediment, effectively trapping suspended particles along the prodelta. The result is a temporary, spatially limited accumulation of local river-derived material within a narrow coastal sector. Notably, the only samples displaying a composition attributable to the Western Alps (Amorosi et al., 2022) are those collected most offshore and unaffected by the 2022 flood. In this context, the river-borne sediment appears deflected and hydrodynamically confined by the WACC (Fig. 12). This evidence indicates that even extreme flood events may leave only a subtle and stratigraphic signal confined to the

505 shallow-marine record, raising concern about the detectability of high-magnitude events in shelfal sedimentary archives.

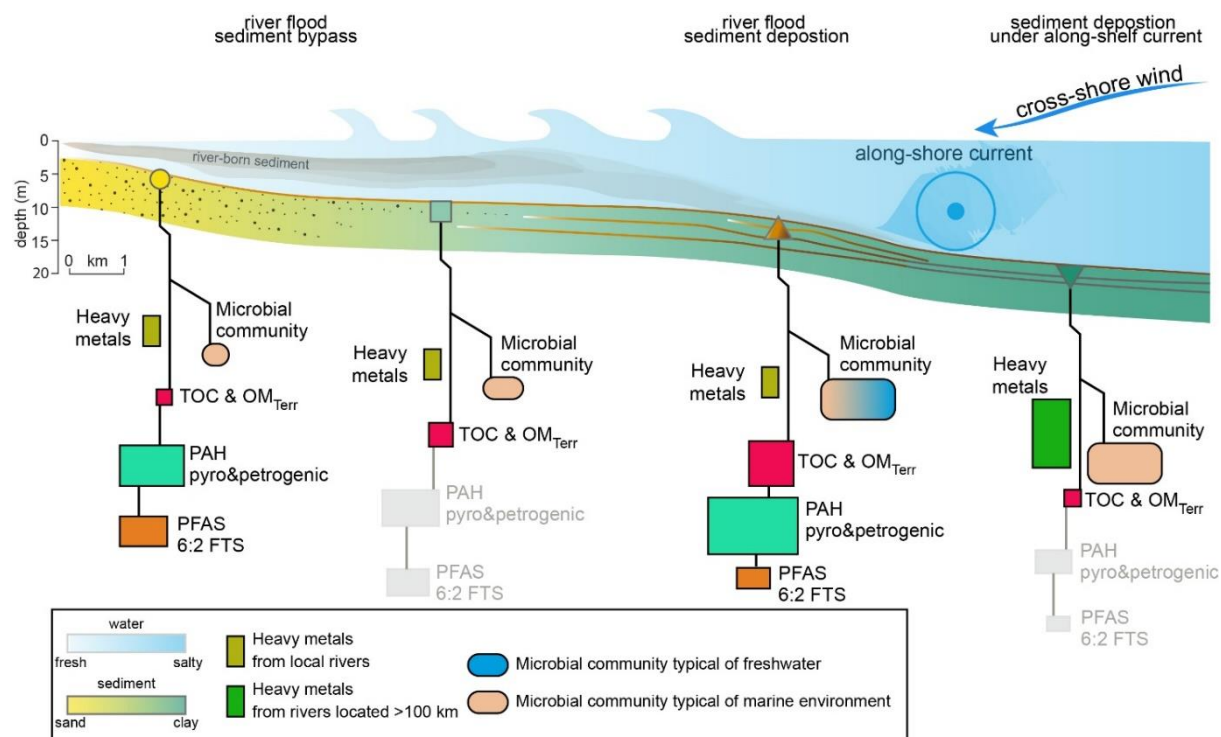


**Figure 12: Conceptual model of sediment transport, contaminant distribution, and microbial community variation along a coastal transect where sediment and associated contaminants are transported and deposited across a coastal gradient under the influence of riverine input, wave action, and along-shelf currents. During flood events, high-energy river flows can bypass the wave-influenced nearshore zone and deliver sediments offshore, where they are preferentially deposited in the prodelta. This distal accumulation occurs in areas where the energy of the plume is reduced and flow is laterally confined by the prevailing along-shelf current. The size of the shapes reflects the relative abundance of each contaminant, while the size of the microbial community symbol reflects diversity rather than quantity. Colors differentiate sources (e.g., local vs. remote rivers) and environmental influences (e.g., fresh vs. salt water).**

## 5.2 River flood deposits and their role in shaping spatial heterogeneity of bacterial communities

The analysis of benthic prokaryotic community composition confirmed that the impact of the September 2022 flood event was not only limited to the nearshore zone, with the impact in the prodelta area appeared to be evident in the most affected rivers





520 (Fig. 12). Variations in substrate composition and grain size shaped both the diversity and structure of microbial assemblages, suggesting that ephemeral depositional events of limited geological significance may have major biological consequences. The lower diversity observed closer to the coast, characterized by higher pollution levels, represents a pattern reported in previous studies, including those conducted in the Adriatic Sea (Quero et al., 2015).

525 The pronounced differences in composition of benthic prokaryotic community along the coast-to-sea transects corroborate the hypothesis of a spatial structuring of sedimentary microbiomes in response to coastal and fluvial inputs. Coastal samples formed a distinct cluster, characterized by higher relative abundances of Thermoanaerobaculaceae and Woeseiaceae, which correlated with the sandy sediment fraction (Fig. 10B). This suggests that coastal microbial communities are closely coupled with sediment granulometry and physicochemical gradients driven by terrestrial inputs (Fagervold et al. 2014; Fazi et al., 2020; Hamamoto et al., 2024), in accordance with previous studies reporting Thermoanaerobaculaceae as ubiquitous in coastal (Fonseca et al., 2022, Giner-Lamia et al., 2024) and disturbed sediments (Ramljak et al., 2024), and Woeseiaceae as cosmopolitan taxon in coastal, organic carbon-rich environments (Hoffmann et al., 2020; Tolar et al., 2020).

Offshore benthic prokaryotic communities exhibited greater heterogeneity and formed two subclusters, reflecting variable levels of exposure to the flood plume and sediment deposition (Figs. 10 and 12). Offshore sediment assemblages in front of the Misa and Esino rivers and C transect appeared more impacted by the flood, supported by their association with higher clay, TOC, and TN levels (Fig. 12). These sites represent major deposition zones, where fine-grained particles transported offshore during the flood settled (Cattaneo et al., 2003; Pellegrini et al., 2015), reshaping the benthic habitat (Fig. 12). Such sedimentation patterns are consistent with the hydrodynamics of the Adriatic Sea, which promotes offshore transport of suspended materials during high-flow events (Langone et al., 2016; Marini et al., 2016).

540 The high relative abundance of Flavobacteriaceae and Vicinamibacteria suggests functional shifts in microbial communities driven by changes in sediment composition and riverine input, as similarly observed in other coastal environments (Quero et al., 2015; Giner-Lamia et al., 2024). The presence of Flavobacteriaceae and other freshwater-indicator taxa (such as Comamonadaceae, Fluviicola ecc.) in the most impacted offshore samples further supports a direct link between river discharge and microbial community restructuring. Differentiation within offshore sediments likely reflects spatial variability in exposure



545 to recent flood-derived deposition, consistent with previous studies highlighting the influence of riverine sedimentation on benthic microbial assemblages (Cibic et al., 2019, Massaccesi et al., 2025). Overall, the reshaping of benthic prokaryotic communities in response to flood-derived sedimentation underscores the need to assess whether such alterations may exert lasting ecological consequences, and whether they ultimately affect the resilience of coastal marine ecosystems.

### 550 **5.3 A broad flood generating spatially restricted pollutant hotspots**

Understanding the origin and behavior of contaminants in marine sediment is crucial for evaluating environmental and human-health risks, as well as for implementing effective coastal management strategies (e.g. Neff et al., 2005; Di Lorenzo et al., 2020; Pizzini et al., 2021; Pellegrini et al., 2023; Trincardi et al., 2023). In this study, we analyzed two classes of priority pollutants -Polycyclic Aromatic Hydrocarbons (PAHs) and Poly- and Perfluorinated Alkyl Substances (PFASs) with particular  
 555 attention to changes following the September 2022 flood event. Overall, PAH concentrations in the analyzed sediments were below the thresholds defined by European regulations, suggesting limited ecotoxicological concern. According to established classification criteria (Baumard et al., 1998), most samples fall into the "low pollution" category ( $<100 \text{ ng g}^{-1} \text{ dw}$ ), except for the Misa 3 sample, which exceeds this threshold and qualifies as "moderate pollution". The spatial distribution of PAHs reveals a heterogeneous pattern shaped by both diffuse and point sources. Elevated concentrations were observed near urban and  
 560 industrialized centers such as Fano, Senigallia, and Ancona, where harbor activities, vehicular traffic, and maritime transport are major contributors. Interestingly, even mountainous areas, typically less impacted by anthropogenic activity, showed detectable levels of PAHs, likely linked to fossil fuel combustion for domestic heating in winter.

The flood of September 2022 significantly influenced these spatial trends by mobilizing and redistributing contaminated sediments across coastal and shelf environments (Fig. 12). North of the most impacted region, samples such as A1, Metauro3,  
 565 and B3 exhibited predominantly petrogenic PAHs (Fig. 8), suggesting inputs from oil-derived sources. In contrast, sediment near the Cesano and Misa river mouths and Site C showed mixed sources, including pyrolytic compounds associated with combustion. Offshore sediments in these areas were enriched in pyrolytic PAHs, indicating strong river-shelf connectivity and highlighting the flood's role in transporting land-derived contaminants seaward. Further south, in the Esino, Musone, and Potenza river systems, PAHs reflected a complex mixture of sources, likely shaped by both input diversity and hydrodynamic



processes such as intense sediment resuspension. Despite the regional extent of the flood, areas north and south of Senigallia showed lower levels of contamination (Fig. 7), emphasizing the highly localized nature of pollutant accumulation. On the contrary, the Misa River, flowing through flood-stricken Senigallia, emerged as a major hotspot for PAH contamination. In contrast to PAHs, the highest PFAS concentrations were found in nearshore sediment immediately adjacent to river mouths (Fig. 12). This pattern highlights a key difference in transport mechanisms: PFASs, unlike traditional persistent organic pollutants (POPs), are not primarily governed by sorption to organic matter. Their surfactant-like properties and amphiphilic structure cause them to interact distinctively with saline environments (e.g. Pan and You, 2010; Jeon et al., 2011; Wang et al., 2013; (Munoz et al., 2017; Newell et al., 2021; Steffen et al., 2021; Li et al., 2022; Yin et al., 2022; Hort et al., 2024). This is especially evident during the 2022 flood event, where PFAS distribution is influenced by mechanisms such as the salting-out effect, a process whereby the solubility of organic compounds decreases as salinity increases. As freshwater from the flood plume mixes with marine waters, compounds like sulfonated fluorotelomers (FTSs) exhibit reduced solubility, resulting in preferential accumulation near the coast. This process has been demonstrated in brackish systems (Hort et al., 2024) and may act as a natural attenuation mechanism limiting PFAS offshore transport. Deeper sediment layers, deposited prior to the 2022 event, showed minimal PFAS concentrations. However, trace amounts of 6:2FTS ( $0.127\text{--}0.355\text{ ng g}^{-1}\text{ dw}$ ) were detected in the northern transects (A, Metauro, B, Cesano), providing a reference for historical contamination potentially related to previous flood or storm events. In surface sediments associated with the 2022 flood, 6:2FTS was the dominant compound, followed by 8:2FTS. These newer-generation PFASs, used as alternatives to banned legacy compounds, are known for their environmental persistence (Field & Seow, 2017). Among traditional PFASs, the most widespread were PFHxA, PFOA, and PFUnA, with peak concentrations in the transect offshore Misa River, confirming the small town of Senigallia as the primary PFAS hotspot. Elevated levels of traditional PFASs were also recorded in the Metauro River transect, likely due to upstream industrial activities (e.g., non-stick cookware manufacturing). Higher copper concentrations in these sediments further support the presence of anthropogenic pressure, although values remained below regulatory limits ( $120\text{ mg kg}^{-1}$ ). This area remains under active environmental monitoring by environmental agencies (e.g. ARPAM) due to its known contamination profile. Summarizing, the spatial and compositional variability of pollutants observed in this study underscores the importance of event-based monitoring strategies. While the 2022 flood had a broad hydrodynamic footprint, its contaminant impact was



595 spatially selective, reinforcing pre-existing gradients rather than creating uniformly distributed pollution. PAHs were redistributed more broadly due to their particulate-bound nature, whereas PFASs remained concentrated in near-source areas due to their solubility and surfactant behavior.

## CONCLUSIONS

600 As climate change accelerates, short-lived extreme events such as river floods are expected to become more frequent and intense. In addition, extreme flood events impact fully anthropogenic environments that have been extensively modified through land-use changes, reduction of permeability, pervasive pollution from industrial plants, transportation, industrialized agriculture and zootechnics and/or urbanization. Consequently, the influence of river floods on coastal dynamics remains insufficiently understood, particularly regarding sediment redistribution, geochemical fluxes, pollutant dispersal, and shifts in  
 605 microbial community. Our study of the 2022 flood event in the Marche region explored the short-term response of an extreme event on a river-dominated mid-latitude coastal system. By integrating sedimentological, geochemical, and biological datasets, we provide a comprehensive picture of the environmental imprint left by a single, high-energy hydrological episode. The September 2022 flood produced a spatially discontinuous and short-lived sedimentary signal in the offshore zone. Most fluvial input were confined to the prodelta, where reduced wave-induced shear stress allowed for temporary deposition of fine-  
 610 grained sediment. However, strong Bora-driven hydrodynamics inhibited offshore propagation, resulting in patchy sediment layers with limited preservation potential. This transient nature poses challenges for the recognition and stratigraphic archiving of extreme flood deposits in marine settings.

Flood-induced sediment heterogeneity also shaped benthic microbial assemblages. In sandy coastal areas, microbial communities were characterized by increased relative abundances of taxa such as Thermoanaerobaculaceae and Woeseiaceae.  
 615 In contrast, the fine-grained, organic-rich prodelta deposits supported diverse prokaryotic communities, including freshwater-derived taxa indicative of recent riverine input. These findings suggest that even ephemeral sedimentary events can alter microbial ecosystem structure along spatial gradients, with potential implications for benthic functioning and biogeochemical cycling.



The analysis of PAHs and PFASs revealed that marine sediment contamination is governed by a complex interplay between chronic anthropogenic pressures and episodic events. The 2022 flood facilitated the redistribution of both traditional and emerging contaminants, with the Misa River and adjacent coastal areas appearing as hotspots of concern. These results reinforce the need for targeted monitoring and remediation strategies, particularly in flood-prone, industrialized coastal regions where contaminant dynamics and concentrations can be highly event-dependent.

Overall, this study underscores the value of multidisciplinary approaches in understanding coastal responses to extreme events. The coupling of sediment transport, hydrodynamics, microbial ecology, and pollutant behavior offers a more complete understanding of how flood events affect the land–sea interface. Recognizing the ephemeral yet impactful nature of such events is essential not only for interpreting recent sedimentary records but also for anticipating future environmental consequences in the Mediterranean and other climatically sensitive coastal systems.

## 630 ACKNOWLEDGMENTS

This project has received funding from the Italian Ministry of Research under the PRIN ON-OFF project contract 2022PMEN2K, and by EU - Next Generation EU Mission 4, Component 2 - CUP B53C22002150006 - Project IR0000032 – ITINERIS - Italian Integrated Environmental Research Infrastructures System. The Authors want to thank Silvio Davolio (CNR-ISAC), Pierluigi Penna (CNR-IRBIM) e Silvia Unguendoli (ARPAE) for respectively MOLOCH, TeleSenigallia, and ADRIAC data provision. Federico Falcini is thanked for sharing orthophoto images.



## REFERENCES

- Adeoba, M. I., Pandelani, T., Ngwangwa, H., & Masebe, T. (2025). The Role of Artificial Intelligence in Sustainable Ocean Waste Tracking and Management: A Bibliometric Analysis. *Sustainability*, 17(9), 3912.
- 640 Ainsworth, R. B., Vakarelov, B. K., & Nanson, R. A. (2011). Dynamic spatial and temporal prediction of changes in depositional processes on clastic shorelines: toward improved subsurface uncertainty reduction and management. *AAPG bulletin*, 95(2), 267-297.
- 645 Allan, R. P., & Soden, B. J. (2008). Atmospheric warming and the amplification of precipitation extremes. *Science*, 321(5895), 1481-1484. Anthony, E., Syvitski, J., Zăinescu, F., Nicholls, R. J.,
- Amorosi, A., & Sammartino, I. (2007). Influence of sediment provenance on background values of potentially toxic metals from near-surface sediments of Po coastal plain (Italy). *International journal of earth sciences*, 96(2), 389-396.
- 650 Amorosi, A., Guermandi, M., Marchi, N., & Sammartino, I. (2014). Fingerprinting sedimentary and soil units by their natural metal contents: a new approach to assess metal contamination. *Science of the Total Environment*, 500, 361-372.
- 655 Amorosi, A., Sammartino, I., Dinelli, E., Campo, B., Guercia, T., Trincardi, F., & Pellegrini, C. (2022). Provenance and sediment dispersal in the Po-Adriatic source-to-sink system unraveled by bulk-sediment geochemistry and its linkage to catchment geology. *Earth-Science Reviews*, 234, 104202.
- Anthony, E. J., Marriner, N., & Morhange, C. (2014). Human influence and the changing geomorphology of Mediterranean deltas and coasts over the last 6000 years: From progradation to destruction phase?. *Earth-Science Reviews*, 139, 336-361.
- 660 Anthony, E., Syvitski, J., Zăinescu, F., Nicholls, R. J., Cohen, K. M., Marriner, N., ... & Maselli, V. (2024). Delta sustainability from the Holocene to the Anthropocene and envisioning the future. *Nature Sustainability*, 7(10), 1235-1246.
- 665 Arienzo, M., Donadio, C., Mangoni, O., Bolinesi, F., Stanislao, C., Trifuoggi, M., Toscanesi, M., Di Natale, G., Ferrara, L., 2017. Characterization and source apportionment of polycyclic aromatic hydrocarbons (pahs) in the sediments of gulf of Pozzuoli (Campania, Italy). *Marine pollution bulletin* 124, 480-487. <http://dx.doi.org/10.1016/j.marpolbul.2017.07.006>
- 670 Bao, R., McIntyre, C., Zhao, M., Zhu, C., Kao, S. J., & Eglinton, T. I. (2016). Widespread dispersal and aging of organic carbon in shallow marginal seas. *Geology*, 44(10), 791-794.
- Bao, R., van der Voort, T. S., Zhao, M., Guo, X., Montluçon, D. B., McIntyre, C., & Eglinton, T. I. (2018). Influence of hydrodynamic processes on the fate of sedimentary organic matter on continental margins. *Global Biogeochemical Cycles*, 32(9), 1420-1432.
- 675 Basili, M., Campanelli, A., Frapiccini, E., Luna, G. M., & Quero, G. M. (2021). Occurrence and distribution of microbial pollutants in coastal areas of the Adriatic Sea influenced by river discharge. *Environmental Pollution*, 285, 117672.
- Baumard, P.; Budzinski, H.; Garrigues, P. Polycyclic aromatic hydrocarbons in sediments and mussels of the western Mediterranean Sea. *Environ. Toxicol. Chem. Int. J.* 1998, 17, 765-776.
- 680 Benincasa, M., Falcini, F., Adduce, C., Sannino, G., & Santoleri, R. (2019). Synergy of satellite remote sensing and numerical ocean modelling for coastal geomorphology diagnosis. *Remote Sensing*, 11(22), 2636.
- Bentley, S. J., & Nittrouer, C. A. (2003). Emplacement, modification, and preservation of event strata on a flood-dominated continental shelf: Eel shelf, Northern California. *Continental Shelf Research*, 23(16), 1465-1493.





- Bhattacharya, J. P., & MacEachern, J. A. (2009). Hyperpynal rivers and prodeltaic shelves in the Cretaceous seaway of North America. *Journal of Sedimentary Research*, 79(4), 184-209.
- Bianchi, T. S., Morrison, E., Barry, S., Arellano, A. R., Feagin, R. A., Hinson, A., ... & Oviedo-Vargas, D. (2018). The fate and transport of allochthonous blue carbon in divergent coastal systems. In *A blue carbon primer* (pp. 27-49). CRC Press.
- Bisci, G. Cantalamessa, G.M. Luna, E. Manini, E. Frapiccini, F. Spagnoli, M. Tramontana, G. Scaella, S. Parlani, M. Sinigaglia, G. Forchielli, F. Mazzoli, D. Magnoni, C. Bellino, D. Pemini., 2021. Qualità dei sedimenti di retro scogliera nelle Marche. Studi costieri 2021 - 29: 29 – 28
- Blöschl, G., Hall, J., Parajka, J., Perdigão, R. A., Merz, B., Arheimer, B., ... & Živković, N. (2017). Changing climate shifts timing of European floods. *Science*, 357(6351), 588-590.
- Blott, S. J., & Pye, K. (2001). GRADISTAT: a grain size distribution and statistics package for the analysis of unconsolidated sediments. *Earth surface processes and Landforms*, 26(11), 1237-1248.
- Blum, M. D., & Roberts, H. H. (2009). Drowning of the Mississippi Delta due to insufficient sediment supply and global sea-level rise. *Nature geoscience*, 2(7), 488-491.
- Bolan, L.P. Padhye, T. Jasemizad, M. Govarthan, N. Karmegam, H. Wijesekara, D. Amarasiri, D. Hou, P. Zhou, B.K. Biswal, R. Balasubramanian, H. Wang, K.H.M. Siddique, J. Rinklebe, M.B. Kirkham, N. Bolan, 2024. Impacts of climate change on the fate of contaminants through extreme weather events, Science of The Total Environment, 909, 168388, <https://doi.org/10.1016/j.scitotenv.2023.168388>.
- Book, J. W., R. P. Signell, and H. Perkins (2007), Measurements of storm and nonstorm circulation in the northern Adriatic: October 2002 through April 2003, *J. Geophys. Res.*, 112, C11S92, doi: [10.1029/2006JC003556](https://doi.org/10.1029/2006JC003556).
- Bosman, A., Romagnoli, C., Madricardo, F., Correggiari, A., Remia, A., Zubalich, R., ... & Trincardi, F. (2020). Short-term evolution of Po della Pila delta lobe from time lapse high-resolution multibeam bathymetry (2013–2016). *Estuarine, Coastal and Shelf Science*, 233, 106533.
- Bouloubassi, I., Roussiez, V., Azzoug, M., & Lorre, A. (2012). Sources, dispersal pathways and mass budget of sedimentary polycyclic aromatic hydrocarbons (PAH) in the NW Mediterranean margin, Gulf of Lions. *Marine Chemistry*, 142, 18-28.
- Bue, G. L., Musa, M., Marchini, A., Riccardi, M. P., Dubois, S. F., Lisco, S., ... & Mancin, N. (2025). Microplastic pollution in the littoral environment: insights from the largest Mediterranean Sabellaria spinulosa (Annelida) reef and shoreface sediments. *Marine Pollution Bulletin*, 217, 118132.
- Bressan, L., Valentini, A., Paccagnella, T., Montani, A., Marsigli, C., and Tesini, M. S.: Sensitivity of sea-level forecasting to the horizontal resolution and sea surface forcing for different configurations of an oceanographic model of the Adriatic Sea, *Adv. Sci. Res.*, 14, 77–84, <https://doi.org/10.5194/asr-14-77-2017>, 2017.
- Callahan, B. J., McMurdie, P. J., Rosen, M. J., Han, A. W., Johnson, A. J. A., & Holmes, S. P. (2016). DADA2: High-resolution sample inference from Illumina amplicon data. *Nature methods*, 13(7), 581-583.
- Campanelli, A., Grilli, F., Paschini, E., & Marini, M. (2011). The influence of an exceptional Po River flood on the physical and chemical oceanographic properties of the Adriatic Sea. *Dynamics of Atmospheres and Oceans*, 52(1-2), 284-297.
- Cattaneo, A., Trincardi, F., Asioli, A., & Correggiari, A. (2007). The Western Adriatic shelf clinoform: energy-limited bottomset. *Continental Shelf Research*, 27(3-4), 506-525.



- 730 Cibic, T., Fazi, S., Nasi, F., Pin, L., Alvisi, F., Berto, D., & Del Negro, P. (2019). Natural and anthropogenic disturbances shape benthic phototrophic and heterotrophic microbial communities in the Po River Delta system. *Estuarine, Coastal and Shelf Science*, 222, 168-182.
- 735 Coleman, J. M., & Wright, L. D. (1975). Modern river deltas: variability of processes and sand bodies. *Houston Geological Society*, 99-149.
- Cohen, K. M., Marriner, N., & Maselli, V. (2024). Delta sustainability from the Holocene to the Anthropocene and envisioning the future. *Nature Sustainability*, 7(10), 1235-1246.
- 740 Gardner, J., Pavelsky, T., Topp, S., Yang, X., Ross, M. R., & Cohen, S. (2023). Human activities change suspended sediment concentration along rivers. *Environmental Research Letters*, 18(6), 064032.
- Cohen, S., Syvitski, J., Ashley, T., Lammers, R., Fekete, B., & Li, H. Y. (2022). Spatial trends and drivers of bedload and suspended sediment fluxes in global rivers. *Water resources research*, 58(6), e2021WR031583.
- 745 Davolio S, Henin R, Stocchi P, Buzzi A. 2017. Bora wind and heavy persistent precipitation: a tmospheric water balance and role of air-sea fluxes over the Adriatic Sea. *Q J R Meteorol Soc.* 143(703):1165–1177.
- De Lucia, C., Amaddii, M., & Arrighi, C. (2024). Tangible and intangible ex post assessment of flood-induced damage to cultural heritage. *Natural Hazards and Earth System Sciences*, 24(12), 4317-4339.
- 750 T. Di Lorenzo, G.C. Hose, D.M.P. Galassi, Assessment of different contaminants in freshwater: origin, fate and ecological impact. *Water* 12(6), 1810 (2020). <https://doi.org/10.3390/w12061810>
- 755 Dinelli, E., Lucchini, F., Fabbri, M., & Cortecci, G. (2001). Metal distribution and environmental problems related to sulfide oxidation in the Libiola copper mine area (Ligurian Apennines, Italy). *Journal of Geochemical Exploration*, 74(1-3), 141-152.
- Dinelli, E., Lucchini, F., Mordenti, A., & Paganelli, L. (1999). Geochemistry of Oligocene–Miocene sandstones of the northern Apennines (Italy) and evolution of chemical features in relation to provenance changes. *Sedimentary Geology*, 127(3-4), 193-207.
- 760 Donnini, M., Santangelo, M., Gariano, S. L., Bucci, F., Peruccacci, S., Alvioli, M., ... & Fiorucci, F. (2023). Landslides triggered by an extraordinary rainfall event in Central Italy on September 15, 2022. *Landslides*, 20(10), 2199-2211.
- 765 Dottori, F., Mentaschi, L., Bianchi, A., Alfieri, L., & Feyen, L. (2023). Cost-effective adaptation strategies to rising river flood risk in Europe. *Nature Climate Change*, 13(2), 196-202.
- Fagervold, S. K., Bourgeois, S., Pruski, A. M., Charles, F., Kerherve, P., Vétion, G., & Galand, P. E. (2014). River organic matter shapes microbial communities in the sediment of the Rhône prodelta. *The ISME journal*, 8(11), 2327-2338.
- 770 Fain, A. M. V., Ogston, A. S., & Sternberg, R. W. (2007). Sediment transport event analysis on the western Adriatic continental shelf. *Continental Shelf Research*, 27(3-4), 431-451.
- 775 Falcini, F., Khan, N. S., Macelloni, L., Horton, B. P., Lutken, C. B., McKee, K. L., ... & Jerolmack, D. J. (2012). Linking the historic 2011 Mississippi River flood to coastal wetland sedimentation. *Nature Geoscience*, 5(11), 803-807.
- M. Fanelli, S. Illuminati, A. Annibaldi, R. De Marco, C. Cerotti, F. Girolametti, B. Ajdini, C. Truzzi, E. Frapiccini, A. Gallerani, M. Tramontana, G. Baldelli, F. Spagnoli, 2025. Mercury historical signature in the Central and Southern Adriatic Sea sediment cores, *Estuarine, Coastal and Shelf Science*, 314, 109144, <https://doi.org/10.1016/j.ecss.2025.109144>.



- 780 Fanelli, M., Illuminati, S., Annibaldi, A., De Marco, R., Cerotti, C., Girolametti, F., ... & Spagnoli, F. (2025). Mercury historical signature in the Central and Southern Adriatic Sea sediment cores. *Estuarine, Coastal and Shelf Science*, 314, 109144.
- Fazi, S., Baldassarre, L., Cassin, D., Quero, G. M., Pizzetti, I., Cibic, T., ... & Del Negro, P. (2020). Prokaryotic community composition and distribution in coastal sediments following a Po river flood event (northern Adriatic Sea, Italy). *Estuarine, Coastal and Shelf Science*, 233, 106547.
- 785 Field, J. A., & Seow, J. (2017). Properties, occurrence, and fate of fluorotelomer sulfonates. *Critical Reviews in Environmental Science and Technology*, 47(8), 643-691.
- 790 Fonseca, A., Espinoza, C., Nielsen, L. P., Marshall, I. P., & Gallardo, V. A. (2022). Bacterial community of sediments under the eastern boundary current system shows high microdiversity and a latitudinal spatial pattern. *Frontiers in Microbiology*, 13, 1016418.
- Fowler, H. J., Lenderink, G., Prein, A. F., Westra, S., Allan, R. P., Ban, N., ... & Zhang, X. (2021). Anthropogenic intensification of short-duration rainfall extremes. *Nature Reviews Earth & Environment*, 2(2), 107-122.
- 795 Franzini, M., Leoni, L., & Saitta, M. (1972). A simple method to evaluate the matrix effects in X-Ray fluorescence analysis. *X-ray Spectrometry*, 1(4), 151-154.
- Franzini, M., Leoni, L., & Saitta, M. (1975). *Revisione di una metodologia analitica per fluorescenza-X, basata sulla correzione completa degli effetti di matrice*. Rendiconti della Società Italiana di Mineralogia e Petrologia, 31, 365-378
- 800 E. Frapiccini, R. De Marco, F. Grilli, M. Marini, A. Annibaldi, E. Prezioso, M. Tramontana, F. Spagnoli, 2024. Anthropogenic contribution, transport, and accumulation of Polycyclic Aromatic Hydrocarbons in sediments of the continental shelf and slope in the Mediterranean Sea, *Chemosphere*, 352, 141285. <https://doi.org/10.1016/j.chemosphere.2024.141285>
- Friedrichs, C. T., & Scully, M. E. (2007). Modeling deposition by wave-supported gravity flows on the Po River prodelta: from seasonal floods to prograding clinoforms. *Continental Shelf Research*, 27(3-4), 322-337.
- 805 Gardner, J., Pavelsky, T., Topp, S., Yang, X., Ross, M. R., & Cohen, S. (2023). Human activities change suspended sediment concentration along rivers. *Environmental Research Letters*, 18(6), 064032.
- Giner-Lamia, J., & Huerta-Cepas, J. (2024). Exploring the sediment-associated microbiota of the Mar Menor coastal lagoon. *Frontiers in Marine Science*, 11, 1319961.
- 810 Goodbred Jr, S. L. (2003). Response of the Ganges dispersal system to climate change: a source-to-sink view since the last interstade. *Sedimentary Geology*, 162(1-2), 83-104.
- Gomez, B., Mertes, L. A., Phillips, J. D., Magilligan, F. J., & James, L. A. (1995). Sediment characteristics of an extreme flood: 1993 upper Mississippi River valley. *Geology*, 23(11), 963-966.
- 815 Govindaraju, K. (1989). 1989 compilation of working values and sample description for 272 geostandards. *Geostandards Newsletter*, 13, 1-113.
- Gruca-Rokosz, R., Cieřła, M., Kida, M., & Ignatowicz, K. (2025). Spatio-Temporal Patterns of Polycyclic Aromatic Hydrocarbons and Phthalates Deposition in Sediments of Reservoirs: Impact of Some Environmental Factors. *Water*, 17(5), 641.
- 820 Gupta, D., Hazarika, B. B., Berlin, M., Sharma, U. M., & Mishra, K. (2021). Artificial intelligence for suspended sediment load prediction: a review. *Environmental earth sciences*, 80(9), 346.



- 825 Hamamoto, K., Mizuyama, M., Nishijima, M., Maeda, A., Gibu, K., Polisen, A., ... & Reimer, J. D. (2024). Diversity, composition and potential roles of sedimentary microbial communities in different coastal substrates around subtropical Okinawa Island, Japan. *Environmental Microbiome*, 19(1), 54.
- 830 Haq, B., & Milliman, J. (2023). Perilous future for river deltas. *GSA Today*, 33(10), 4-12.
- Harris, C. K., Sherwood, C. R., Signell, R. P., Bever, A. J., & Warner, J. C. (2008). Sediment dispersal in the northwestern Adriatic Sea. *Journal of Geophysical Research: Oceans*, 113(C11).
- 835 Hoffmann, K., Bienhold, C., Buttigieg, P. L., Knittel, K., Laso-Pérez, R., Rapp, J. Z., ... & Offre, P. (2020). Diversity and metabolism of Woeseiales bacteria, global members of marine sediment communities. *The ISME journal*, 14(4), 1042-1056.
- Hood, W. G. (2010). Tidal channel meander formation by depositional rather than erosional processes: examples from the prograding Skagit River Delta (Washington, USA). *Earth Surface Processes and Landforms: The Journal of the British Geomorphological Research Group*, 35(3), 319-330.
- 840 Hort, H. M., Robinson, C. E., Sawyer, A. H., Li, Y., Cardoso, R., Lee, S. A., ... & Newell, C. J. (2024). Conceptualizing controlling factors for PFAS salting out in groundwater discharge zones along sandy beaches. *Groundwater*, 62(6), 860-875.
- 845 IPCC, 2021, Climate Change 2021: The Physical Science Basis. Contribution of Working Group I to the Sixth Assessment Report of the Intergovernmental Panel on Climate Change: Cambridge, UK, and New York, Cambridge University Press, 2391 p., <https://doi.org/10.1017/9781009157896>.
- Jaramillo, S., Sheremet, A., Allison, M. A., Reed, A. H., & Holland, K. T. (2009). Wave-mud interactions over the muddy Atchafalaya subaqueous clinoform, Louisiana, United States: Wave-supported sediment transport. *Journal of Geophysical Research: Oceans*, 114(C4).
- 850 Jeon, J., Kannan, K., Lim, B. J., An, K. G., & Kim, S. D. (2011). Effects of salinity and organic matter on the partitioning of perfluoroalkyl acid (PFAs) to clay particles. *Journal of Environmental Monitoring*, 13(6), 1803-1810.
- 855 Jolaosho, T. L., Rasak, M. F., Omotoye, E. V., Araomo, O. V., Adekoya, O. S., Abolaji, O. Y., & Hungbo, J. J. (2025). Microplastics in freshwater and marine ecosystems: Occurrence, characterization, sources, distribution dynamics, fate, transport processes, potential mitigation strategies, and policy interventions. *Ecotoxicology and Environmental Safety*, 294, 118036.
- 860 Korus, J. T., & Fielding, C. R. (2015). Asymmetry in Holocene river deltas: patterns, controls, and stratigraphic effects. *Earth-Science Reviews*, 150, 219-242.
- Kundzewicz, Z. W., Kanae, S., Seneviratne, S. I., Handmer, J., Nicholls, N., Peduzzi, P., ... & Sherstyukov, B. (2014). Flood risk and climate change: global and regional perspectives. *Hydrological Sciences Journal*, 59(1), 1-28.
- 865 Kundzewicz, Z. W., Pińskwar, I., & Brakenridge, G. R. (2018). Changes in river flood hazard in Europe: a review. *Hydrology research*, 49(2), 294-302.
- 870 Langone, L., et al. Dynamics of particles along the western margin of the Southern Adriatic: Processes involved in transferring particulate matter to the deep basin. *Marine Geology*, 2016, 375: 28-43
- Leoni, L., & Saitta, M. (1976). Determination of yttrium and niobium on standard silicate rocks by X-ray fluorescence analyses. *X-ray Spectrometry*, 5(1), 29-30.



- 875 Leoni, L., Menichini, M., & Saitta, M. (1982). Determination of S, Cl and F in silicate rocks by X-Ray fluorescence analyses. *X-Ray Spectrometry*, 11(4), 156-158.
- Li, C., Zhang, C., Gibbes, B., Wang, T., & Lockington, D. (2022). Coupling effects of tide and salting-out on perfluorooctane sulfonate (PFOS) transport and adsorption in a coastal aquifer. *Advances in Water Resources*, 166, 104240.
- 880 Liu, J. P., Li, A. C., Xu, K. H., Velozzi, D. M., Yang, Z. S., Milliman, J. D., & DeMaster, D. J. (2006). Sedimentary features of the Yangtze River-derived along-shelf clinoform deposit in the East China Sea. *Continental Shelf Research*, 26(17-18), 2141-2156.
- Lee, C.C., Chen, C.S., Wang, Z.X., Tien, C.J., 2021. Polycyclic aromatic hydrocarbons in 30 river ecosystems, Taiwan: sources, and ecological and human health risks. *Sci. Total Environ.* 795, 1–14.  
 885 <https://doi.org/10.1016/j.scitotenv.2021.148867>.
- Lehmann, J., Coumou, D., & Frieler, K. (2015). Increased record-breaking precipitation events under global warming. *Climatic Change*, 132, 501-515.
- Lim, K. Y., Zakaria, N. A., & Foo, K. Y. (2021). Geochemistry pollution status and ecotoxicological risk assessment of heavy metals in the Pahang River sediment after the high magnitude of flood event. *Hydrology Research*, 52(1), 107-124.
- 890 Lohrenz, S. E., Dagg, M. J., & Whitledge, T. E. (1990). Enhanced primary production at the plume/oceanic interface of the Mississippi River. *Continental shelf research*, 10(7), 639-664.
- Lucchini F., Frignani M., Sammartino I., Dinelli E., Bellucci L.G. (2001). Composition of Venice Lagoon sediments: distribution, sources, settings and recent evolution. *GeoActa* 1, 7-20.
- 895 Macquaker, J. H., Bentley, S. J., & Bohacs, K. M. (2010). Wave-enhanced sediment-gravity flows and mud dispersal across continental shelves: Reappraising sediment transport processes operating in ancient mudstone successions. *Geology*, 38(10), 947-950.
- Maletić, S.P., Beljin, J.M., Roñcević, S.D., Grgić, M.G., Dalmacija, B.D., 2019. State of the art and future challenges for polycyclic aromatic hydrocarbons in sediments: sources, fate, bioavailability and remediation techniques. *J. Hazard Mater.* 365, 467–482. <https://doi.org/10.1016/j.jhazmat.2018.11.020>.
- 900 Mali, M., Ragone, R., Dell'Anna, M.M., Romanazzi, G., Damiani, L., Mastorilli, P., 2022. Improved identification of pollution source attribution by using PAH ratios combined with multivariate statistics. *Sci. Rep.* 12, 1–13. <https://doi.org/10.1038/s41598-022-23966-4>.
- 905 Marini, M., Maselli, V., Campanelli, A., Foglini, F., & Grilli, F. (2016). Role of the Mid-Adriatic deep in dense water interception and modification. *Marine Geology*, 375, 5-14.
- Martin, M. (2011). Cutadapt removes adapter sequences from high-throughput sequencing reads. *EMBnet journal*, 17(1), 10-12.
- 910 Massaccesi, N., Basili, M., Coci, M., Cassin, D., Zonta, R., Manini, E., ... & Quero, G. M. (2025). Benthic prokaryotic diversity in Po River Delta lagoons (North Adriatic Sea) is shaped by riverine freshwater inputs. *Estuarine, Coastal and Shelf Science*, 109348.
- 915 Mayer, L. M. (1994). Surface area control of organic carbon accumulation in continental shelf sediments. *Geochimica et Cosmochimica Acta*, 58(4), 1271-1284.
- McMurdie, P. J., & Holmes, S. (2013). phyloseq: an R package for reproducible interactive analysis and graphics of microbiome census data. *PloS one*, 8(4), e61217.
- 920





- Mead, R. N., & Goñi, M. A. (2008). Matrix protected organic matter in a river dominated margin: A possible mechanism to sequester terrestrial organic matter?. *Geochimica et Cosmochimica Acta*, 72(11), 2673-2686.
- 925 Merz, B., Blöschl, G., Vorogushyn, S., Dottori, F., Aerts, J. C., Bates, P., ... & Macdonald, E. (2021). Causes, impacts and patterns of disastrous river floods. *Nature Reviews Earth & Environment*, 2(9), 592-609.
- Milliman, J. D., & Syvitski, J. P. (1992). Geomorphic/tectonic control of sediment discharge to the ocean: the importance of small mountainous rivers. *The journal of Geology*, 100(5), 525-544.
- 930 MSFD, 2008. Directive 2008/56/EC of the European Parliament and of the Council establishing a framework for community action in the field of marine environmental policy (Marine Strategy Framework Directive). OJ L 164, 25.6.2008, p. 19–40.
- Munoz, G., Budzinski, H., & Labadie, P. (2017). Influence of environmental factors on the fate of legacy and emerging per- and polyfluoroalkyl substances along the salinity/turbidity gradient of a macrotidal estuary. *Environmental science & technology*, 51(21), 12347-12357.
- 935 Neff, J.M., Stout, S.A., Gunster, D.G., 2005. Ecological risk assessment of polycyclic aromatic hydrocarbons in sediments: identifying sources and ecological hazard. *Integr Environ Asses* 1, 22–23. [https://doi.org/10.1897/IEAM\\_2004a-016.1](https://doi.org/10.1897/IEAM_2004a-016.1).
- Nie, J., Sobel, A. H., Shaevitz, D. A., & Wang, S. (2018). Dynamic amplification of extreme precipitation sensitivity. *Proceedings of the National Academy of Sciences*, 115(38), 9467-9472.
- 940 Nikki, R., Jaleel, K. A., Razaque, M. A., Gupta, P., Rathore, C., Saha, M., ... & Kumar, T. G. (2025). Assessment of hazardous microplastic polymers and phthalic acid esters in an invasive mollusk (*Mytella strigata*) from the Cochin estuary, southwest coast of India: Unraveling ecosystem risks. *Science of The Total Environment*, 967, 178798.
- 945 Nittrouer, C. A., Kuehl, S. A., DeMaster, D. J., & Kowsmann, R. O. (1986). The deltaic nature of Amazon shelf sedimentation. *Geological Society of America Bulletin*, 97(4), 444-458.
- Oksanen, J., Simpson, G. L., Blanchet, F. G., Kindt, R., Legendre, P., Minchin, P. R., ... & Weedon, J. (2001). *Vegan: community ecology package. (No Title)*.
- 950 Overeem, I., & Brakenridge, R. G. (Eds.). (2009). *Dynamics and vulnerability of delta systems* (Vol. 35). GKSS Research Centre, LOICZ Internat. Project Office, Inst. for Coastal Research.
- Owowenu, E. K., Nnadozie, C. F., Akamagwuna, F., Siwe-Noundou, X., & Odume, O. N. (2025). Occurrence and distribution of microplastics in functionally delineated hydraulic zones in selected Rivers, Eastern Cape, South Africa. *Environmental Pollution*, 126544.
- 955 Palinkas, C. M., & Nittrouer, C. A. (2006). Clinoform sedimentation along the Apennine shelf, Adriatic Sea. *Marine Geology*, 234(1-4), 245-260.
- Palinkas, C. M., & Nittrouer, C. A. (2007). Modern sediment accumulation on the Po shelf, Adriatic Sea. *Continental Shelf Research*, 27(3-4), 489-505.
- Pan, G., & You, C. (2010). Sediment–water distribution of perfluorooctane sulfonate (PFOS) in Yangtze River Estuary. *Environmental pollution*, 158(5), 1363-1367.
- 960 Patruno, S., & Helland-Hansen, W. (2018). Clinoforms and clinoform systems: Review and dynamic classification scheme for shorelines, subaqueous deltas, shelf edges and continental margins. *Earth-Science Reviews*, 185, 202-233.





- Peng, Y., Yu, Q., Du, Z., Wang, L., Wang, Y., & Gao, S. (2022). Gravity-driven sediment flows on the shallow sea floor of a muddy open coast. *Marine Geology*, 445, 106759.
- 965 Pellegrini, C., Sammartino, I., Schieber, J., Tesi, T., Paladini de Mendoza, F., Rossi, V., & Amorosi, A. (2024). On depositional processes governing along-strike facies variations of fine-grained deposits: Unlocking the Little Ice Age subaqueous clinothems on the Adriatic shelf. *Sedimentology*, 71(3), 941-973.
- Pellegrini, C., Saliu, F., Bosman, A., Sammartino, I., Raguso, C., Mercorella, A., & Rovere, M. (2023). Hotspots of microplastic accumulation at the land-sea transition and their spatial heterogeneity: The Po River prodelta (Adriatic Sea). *Science of The Total Environment*, 895, 164908.
- 970 Pellegrini, C., Tesi, T., Schieber, J., Bohacs, K. M., Rovere, M., Asioli, A., & Trincardi, F. (2021). Fate of terrigenous organic carbon in muddy clinothems on continental shelves revealed by stratal geometries: Insight from the Adriatic sedimentary archive. *Global and Planetary Change*, 203, 103539.
- Pellegrini, C., Patruno, S., Helland-Hansen, W., Steel, R. J., & Trincardi, F. (2020). Clinoforms and clinothems: Fundamental elements of basin infill. *Basin Research*, 32(Clinoforms and Clinothems: Fundamental Elements of Basin Infill), 187-205.
- 975 Pellegrini, C., Maselli, V., Cattaneo, A., Piva, A., Ceregato, A., & Trincardi, F. (2015). Anatomy of a compound delta from the post-glacial transgressive record in the Adriatic Sea. *Marine Geology*, 362, 43-59.
- Pierdomenico, M., Ridente, D., Casalbore, D., Di Bella, L., Milli, S., & Chiocci, F. L. (2022). Plastic burial by flash-flood deposits in a prodelta environment (Gulf of Patti, Southern Tyrrhenian Sea). *Marine Pollution Bulletin*, 181, 113819.
- 980 Pitarch, J., Falcini, F., Nardin, W., Brando, V. E., Di Cicco, A., & Marullo, S. (2019). Linking flow-stream variability to grain size distribution of suspended sediment from a satellite-based analysis of the Tiber River plume (Tyrrhenian Sea). *Scientific reports*, 9(1), 19729.
- Pizzini, S., Giubilato, E., Morabito, E., Barbaro, E., Bonetto, A., Calgaro, L., ... & Marcomini, A. (2024). Contaminants of emerging concern in water and sediment of the Venice Lagoon, Italy. *Environmental Research*, 249, 118401.
- 985 Pizzini, S., Morabito, E., Gregoris, E., Vecchiato, M., Corami, F., Piazza, R., & Gambaro, A. (2021). Occurrence and source apportionment of organic pollutants in deep sediment cores of the Venice Lagoon. *Marine Pollution Bulletin*, 164, 112053.
- Pomaro, A., Cavaleri, L. & Lionello, P. Climatology and trends of the Adriatic Sea wind waves: analysis of a 37-year long instrumental data set. *International Journal of Climatology* 37(12), 4237–4250 (2017).
- Poulain, P. M. (2001). Adriatic Sea surface circulation as derived from drifter data between 1990 and 1999. *Journal of Marine Systems*, 29(1-4), 3-32.
- 990 Puig, P., Ogston, A. S., Guillén, J., Fain, A. M. V., & Palanques, A. (2007). Sediment transport processes from the topset to the foreset of a crenulated clinoform (Adriatic Sea). *Continental Shelf Research*, 27(3-4), 452-474.
- Pulvirenti, L., Squicciarino, G., Fiori, E., Candela, L., & Puca, S. (2023). Analysis and processing of the COSMO-SkyMed second generation images of the 2022 marche (Central Italy) flood. *Water*, 15(7), 1353.
- 995 Quero, G. M., Cassin, D., Botter, M., Perini, L., & Luna, G. M. (2015). Patterns of benthic bacterial diversity in coastal areas contaminated by heavy metals, polycyclic aromatic hydrocarbons (PAHs) and polychlorinated biphenyls (PCBs). *Frontiers in microbiology*, 6, 1053.
- Ramljak, A., Žučko, J., Lučić, M., Babić, I., Morić, Z., Fafandel, M., ... & Petrić, I. (2024). Microbial communities as indicators of marine ecosystem health: Insights from coastal sediments in the eastern Adriatic Sea. *Marine pollution bulletin*, 205, 116649.
- 1000



- Ranjbar Jafarabadi, A., Riyahi Bakhtiari, A., Shadmehri Toosi, A., 2017. Comprehensive and comparative ecotoxicological and human risk assessment of polycyclic aromatic hydrocarbons (PAHs) in reef surface sediments and coastal seawaters of Iranian Coral Islands, Persian Gulf. *Ecotoxicol. Environ. Saf.* 145, 640–652. <https://doi.org/10.1016/j.ecoenv.2017.08.016>.
- 1005 Rath, P., Panda, U. C., Bhatta, D., & Sahu, K. C. (2009). Use of sequential leaching, mineralogy, morphology and multivariate statistical technique for quantifying metal pollution in highly polluted aquatic sediments—A case study: Brahmani and Nandira Rivers, India. *Journal of Hazardous materials*, 163(2-3), 632-644.
- Ravaioli, M., Bergami, C., Riminucci, F., Langone, L., Cardin, V., Di Sarra, A., & Crise, A. (2016). The RITMARE Italian Fixed-Point Observatory Network (IFON) for marine environmental monitoring: a case study. *Journal of Operational Oceanography*, 9(sup1), s202-s214.
- 1010 Regione Marche. (2016). Studio sulle analisi ambientali in aria (aggiornato a giugno 2019). Dipartimento di Ingegneria Industriale e Scienze Matematiche, Università Politecnica delle Marche. Ultima consultazione Regione Marche il 20/06/2024.
- Riminucci, F., Funari, V., Ravaioli, M., & Capotondi, L. (2022). Trace metals accumulation on modern sediments from Po river prodelta, North Adriatic Sea. *Marine Pollution Bulletin*, 175, 113399.
- 1015 Roussiez, V., Ludwig, W., Monaco, A., Probst, J. L., Bouloubassi, I., Buscail, R., & Saragoni, G. (2006). Sources and sinks of sediment-bound contaminants in the Gulf of Lions (NW Mediterranean Sea): a multi-tracer approach. *Continental Shelf Research*, 26(16), 1843-1857.
- 1020 Sammartino, I. (2004). Heavy-metal anomalies and bioavailability from soils of southeastern Po Plain. *GeoActa*, 3, 35-42.
- Sanchez-Vidal, A., Higuera, M., Martí, E., Lique, C., Calafat, A., Kerhervé, P., & Canals, M. (2013). Riverine transport of terrestrial organic matter to the North Catalan margin, NW Mediterranean Sea. *Progress in oceanography*, 118, 71-80.
- 1025 Schieber, J. (2013). SEM observations on ion-milled samples of Devonian black shales from Indiana and New York: the petrographic context of multiple pore types.
- Schimmelmann, A., Riese, D. J., & Schieber, J. (2015, March). Fast and economical sampling and resin-embedding technique for small cores of unconsolidated, fine-grained sediment. In *Proceedings of the 2015 Pacific Climate (PACCLIM) Workshop, Asilomar Conference Grounds, Pacific Grove, CA, USA* (pp. 8-11).
- 1030 Sherwood, C. R., Book, J. W., & Harris, C. K. (2015). Sediment dynamics in the Adriatic Sea investigated with coupled models. *Oceanography*, 17(4), 58.
- 1035 Signell, R. P., Chiggiato, J., Horstmann, J., Doyle, J. D., Pullen, J., & Askari, F. (2010). High-resolution mapping of Bora winds in the northern Adriatic Sea using synthetic aperture radar. *Journal of Geophysical Research: Oceans*, 115(C4).
- Simon-Sánchez, L., Grelaud, M., Garcia-Orellana, J., & Ziveri, P. (2019). River Deltas as hotspots of microplastic accumulation: The case study of the Ebro River (NW Mediterranean). *Science of the total environment*, 687, 1186-1196.
- 1040 Slater, L., Villarini, G., Archfield, S., Faulkner, D., Lamb, R., Khouakhi, A., & Yin, J. (2021). Global changes in 20-year, 50-year, and 100-year river floods. *Geophysical Research Letters*, 48(6), e2020GL091824.
- 1045 Steffens, S. D., Cook, E. K., Sedlak, D. L., & Alvarez-Cohen, L. (2021). Under-reporting potential of perfluorooctanesulfonic acid (PFOS) under high-ionic strength conditions. *Environmental Science & Technology Letters*, 8(12), 1032-1037.
- Sun, Q., Zhang, X., Zwiers, F., Westra, S., & Alexander, L. V. (2021). A global, continental, and regional analysis of changes in extreme precipitation. *Journal of Climate*, 34(1), 243-258.



- 1050 Syvitski, J., Ángel, J. R., Saito, Y., Overeem, I., Vörösmarty, C. J., Wang, H., & Olago, D. (2022). Earth's sediment cycle during the Anthropocene. *Nature Reviews Earth & Environment*, 3(3), 179-196.
- Syvitski, J. P., & Kettner, A. J. (2007). On the flux of water and sediment into the Northern Adriatic Sea. *Continental Shelf Research*, 27(3-4), 296-308.
- 1055 Syvitski, J. P., Kettner, A. J., Overeem, I., Hutton, E. W., Hannon, M. T., Brakenridge, G. R., ... & Nicholls, R. J. (2009). Sinking deltas due to human activities. *Nature Geoscience*, 2(10), 681-686.
- Syvitski, J. P., Peckham, S. D., Hilberman, R., & Mulder, T. (2003). Predicting the terrestrial flux of sediment to the global ocean: a planetary perspective. *Sedimentary Geology*, 162(1-2), 5-24.
- 1060 Syvitski, J. P., Vörösmarty, C. J., Kettner, A. J., & Green, P. (2005). Impact of humans on the flux of terrestrial sediment to the global coastal ocean. *science*, 308(5720), 376-380.
- Tesi, T., Langone, L., Giani, M., Ravaioli, M., & Miserocchi, S. (2013). Source, diagenesis, and fluxes of particulate organic carbon along the western Adriatic Sea (Mediterranean Sea). *Marine Geology*, 337, 156-170.
- 1065 Tesi, T., Miserocchi, S., Goni, M. E. A., Langone, L., Boldrin, A., & Turchetto, M. (2007). Organic matter origin and distribution in suspended particulate materials and surficial sediments from the western Adriatic Sea (Italy). *Estuarine, Coastal and Shelf Science*, 73(3-4), 431-446.
- 1070 Tesi, T., Miserocchi, S., Langone, L., Boni, L., & Guerrini, F. (2006). Sources, fate and distribution of organic matter on the western Adriatic continental shelf, Italy. *Water, Air, & Soil Pollution: Focus*, 6(5), 593-603.
- Tolar, B. B., Boye, K., Bobb, C., Maher, K., Bargar, J. R., & Francis, C. A. (2020). Stability of floodplain subsurface microbial communities through seasonal hydrological and geochemical cycles. *Frontiers in Earth Science*, 8, 338.
- 1075 Traykovski, P., Geyer, W. R., Irish, J. D., & Lynch, J. F. (2000). The role of wave-induced density-driven fluid mud flows for cross-shelf transport on the Eel River continental shelf. *Continental shelf research*, 20(16), 2113-2140.
- 1080 Traykovski, P., Wiberg, P. L., & Geyer, W. R. (2007). Observations and modeling of wave-supported sediment gravity flows on the Po prodelta and comparison to prior observations from the Eel shelf. *Continental Shelf Research*, 27(3-4), 375-399.
- Trincardi, F., Amorosi, A., Bosman, A., Correggiari, A., Madricardo, F., & Pellegrini, C. (2020). Ephemeral rollover points and clinotherm evolution in the modern Po Delta based on repeated bathymetric surveys. *Basin Research*, 32(Clinofoms and Clinotherms: Fundamental Elements of Basin Infill), 402-418.
- 1085 Trincardi, F., Francocci, F., Pellegrini, C., d'Alcalà, M. R., & Sprovieri, M. (2023). The Mediterranean Sea in the Anthropocene. In *Oceanography of the Mediterranean Sea* (pp. 501-553). Elsevier.
- 1090 Vona, I., Colella, S., Sammartino, M., Brando, V. E., & Falcini, F. (2025). Positive correlation between the Po River discharge and ocean colour trends of Chl and TSM in the Adriatic Sea. *Frontiers in Remote Sensing*, 6, 1574347.
- Vörösmarty, C. J., Meybeck, M., Fekete, B., Sharma, K., Green, P., & Syvitski, J. P. (2003). Anthropogenic sediment retention: major global impact from registered river impoundments. *Global and planetary change*, 39(1-2), 169-190.
- 1095 Wang, X. H., & Pinardi, N. (2002). Modeling the dynamics of sediment transport and resuspension in the northern Adriatic Sea. *Journal of Geophysical Research: Oceans*, 107(C12), 18-1.



- 1100 Wang, S., Wang, H., & Deng, W. (2013). Perfluorooctane sulfonate (PFOS) distribution and effect factors in the water and sediment of the Yellow River Estuary, China. *Environmental monitoring and assessment*, 185(10), 8517-8524.
- Warner J C, Armstrong B, He R and Zambon J B (2010) Development of a coupled ocean–atmosphere–wave–sediment transport (COAWST) modeling system *Ocean Model*. 35 230–44
- 1105 Warrick, J. A., Buscombe, D., Vos, K., Bryan, K. R., Castelle, B., Cooper, J. A. G., ... & Young, A. P. (2024). Coastal shoreline change assessments at global scales. *Nature communications*, 15(1), 2316.
- Weiss, L., Estournel, C., Marsaleix, P., Mikolajczak, G., Constant, M., & Ludwig, W. (2024). From source to sink: part 1—characterization and Lagrangian tracking of riverine microplastics in the Mediterranean Basin. *Environmental Science and Pollution Research*, 1-24.
- 1110 Wentworth, C. K. (1922). A scale of grade and class terms for clastic sediments. *The journal of geology*, 30(5), 377-392.
- Westra, S., Alexander, L. V., & Zwiers, F. W. (2013). Global increasing trends in annual maximum daily precipitation. *Journal of climate*, 26(11), 3904-3918.
- 1115 Wheatcroft, R. A. (2000). Oceanic flood sedimentation: a new perspective. *Continental Shelf Research*, 20(16), 2059-2066.
- Wheatcroft, R. A., & Drake, D. E. (2003). Post-depositional alteration and preservation of sedimentary event layers on continental margins, I. The role of episodic sedimentation. *Marine Geology*, 199(1-2), 123-137.
- 1120 Wheatcroft, R. A., Goñi, M. A., Hatten, J. A., Pasternack, G. B., & Warrick, J. A. (2010). The role of effective discharge in the ocean delivery of particulate organic carbon by small, mountainous river systems. *Limnology and Oceanography*, 55(1), 161-171.
- 1125 Winsemius, H. C., Aerts, J. C., Van Beek, L. P., Bierkens, M. F., Bouwman, A., Jongman, B., ... & Ward, P. J. (2016). Global drivers of future river flood risk. *Nature Climate Change*, 6(4), 381-385.
- 1130 Yin, C., Pan, C. G., Xiao, S. K., Wu, Q., Tan, H. M., & Yu, K. (2022). Insights into the effects of salinity on the sorption and desorption of legacy and emerging per-and polyfluoroalkyl substances (PFASs) on marine sediments. *Environmental Pollution*, 300, 118957.
- Yunker, M.B., Macdonald, R.W., Vingarzan, R., Mitchell, R.H., Goyette, D., Sylvestre, S., 2002. PAHs in the Fraser River basin: a critical appraisal of PAH ratios as indicators of PAH source and composition. *Organic Geochemistry* 33, 489-515.
- 1135